Title
Role of Species-Specific Primary Structure Differences in Aβ42 Assembly and Neurotoxicity

Journal
ACS Chemical Neuroscience, 6(12)

ISSN
1948-7193

Authors
Roychaudhuri, Robin
Zheng, Xueyun
Lomakin, Aleksey
et al.

Publication Date
2015-12-16

DOI
10.1021/acschemneuro.5b00180

Peer reviewed

ACS Chemical Neuroscience

Research Article

pubs.acs.org/chemneuro

Role of Species-Specific Primary Structure Differences in Aβ42 Assembly and Neurotoxicity

Robin Roychaudhuri,[†] Xueyun Zheng,[‡] Aleksey Lomakin,[§] Panchanan Maiti,[†,⊥] Margaret M. Condron,[†] George B. Benedek,[§] Gal Bitan,[†,∥] Michael T. Bowers,[‡] and David B. Teplow*[,†,∥]

[†]Department of Neurology, David Geffen School of Medicine at UCLA, 635 Charles E. Young Drive South, Room 445, Los Angeles, California, 90095, United States

[‡]Department of Chemistry and Biochemistry, University of California, Santa Barbara, California 93106, United States

[§]Department of Physics and Center for Materials Science and Engineering, Massachusetts Institute of Technology, Cambridge, Massachusetts 02139, United States

[∥]Molecular Biology Institute and Brain Research Institute, University of California, Los Angeles, California 90095, United States

Supporting Information

ABSTRACT: A variety of species express the amyloid β-protein (Aβ (the term "Aβ" refers both to Aβ40 and Aβ42, whereas "Aβ40" and "Aβ42" refer to each isoform specifically). Those species expressing Aβ with primary structure identical to that expressed in humans have been found to develop amyloid deposits and Alzheimer's disease-like neuropathology. In contrast, the Aβ sequence in mice and rats contains three amino acid substitutions, Arg5Gly, His13Arg, and Tyr10Phe, which apparently prevent the development of AD-like neuropathology. Interestingly, the brush-tailed rat, *Octodon degus*, expresses Aβ containing only one of these substitutions, His13Arg, and *does* develop AD-like pathology. We investigate here the biophysical and biological properties of Aβ peptides from humans, mice (*Mus musculus*), and rats (*Octodon degus*). We find that each peptide displays statistical coil → β-sheet secondary structure transitions, transitory formation of hydrophobic surfaces, oligomerization, formation of annuli, protofibrils, and fibrils, and an inverse correlation between rate of aggregation and aggregate size (faster aggregation produced smaller aggregates). The rank order of assembly rate was mouse > rat > Aβ42. The rank order of neurotoxicity of assemblies formed by each peptide immediately after preparation was Aβ42 > mouse ≈ rat. These data do *not* support long-standing hypotheses that the primary factor controlling development of AD-like neuropathology in rodents is Aβ sequence. Instead, the data support a hypothesis that assembly quaternary structure *and* organismal responses to toxic peptide assemblies mediate neuropathogenetic effects. The implication of this hypothesis is that a valid understanding of disease causation within a given system (organism, tissue, etc.) requires the coevaluation of both biophysical and cell biological properties of that system.

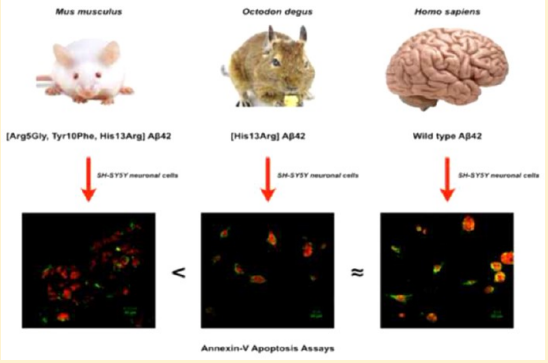

KEYWORDS: *Amyloid β-protein, Alzheimer's disease, aggregation, neurotoxicity, rats, mice, humans*

INTRODUCTION

Alzheimer's disease (AD) is the most common form of late-life dementia.[1] An important working hypothesis of disease causation is aberrant folding and assembly of Aβ42.[2] This assembly leads to the production of extracellular amyloid plaques by the amyloid β-protein (Aβ) and of intracellular neurofibrillary tangles by tau. Such histopathologic findings are pathognomonic for AD and accompany progressive declines in cognitive ability and executive function.[1,3−5] AD pathology also has been observed in dogs, polar bears, rabbits, cows, sheep, pigs, guinea pigs, orangutans, and rhesus monkeys, but until recently it has not been found in mice or rats.[6−8] In 2005, Inestrosa et al.[9,10] reported that the brush-tailed rat, *Octodon degus* (*Od*; a rodent indigenous to Chile), displays both intra- and extracellular deposits of Aβ, intracellular accumulation of phosphorylated tau, strong astrocytic responses, and pyramidal neurons rich in acetylcholinesterase. *Od* naturally develops these neuropathological signs of AD between 12 and 36 months of age. This pathology has been correlated with decreases in spatial and object recognition memory, post-synaptic function, and synaptic plasticity.[11,12] Interestingly, the brains from another rodent, the naked mole rat (the longest lived rodent, with a life span ≈ 32 years) showed levels of Aβ42 similar to a 3X-Tg-AD mouse model of AD.[13]

Examination of the primary structure of Aβ42 in *Od* and in the naked mole rat reveals 100% identity,[13,14] and this amino

Received: July 4, 2015
Revised: September 10, 2015

DOI: 10.1021/acschemneuro.5b00180
ACS Chem. Neurosci. XXXX, XXX, XXX−XXX

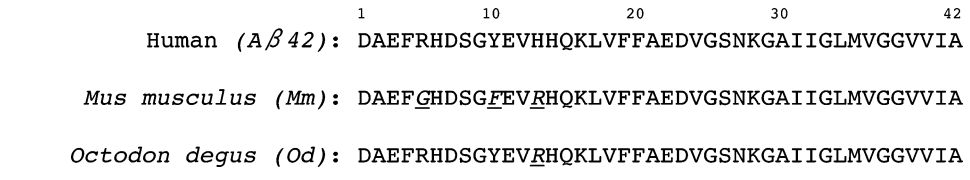

Figure 1. Primary structures of human, *Mm*, and *Od* Aβ42. One-letter amino acid code is used to present the sequences of each Aβ42 peptide. Underlined, italicized letters indicate amino acid differences or substitutions among the peptides.

acid sequence is identical to that of human Aβ42, *except* for a His13Arg substitution (Figure 1). In contrast, mouse (*Mus musculus*; *Mm*) Aβ42 differs from human Aβ42 in having three amino acid substitutions: Arg5Gly, His13Arg, and Tyr10-Phe.[6,15−17] Mutations in the amyloid β-protein precursor (APP) that result in amino acid substitutions at other sites in Aβ cause familial AD and cerebral amyloid angiopathy (CAA).[1] It is interesting that an identical amino acid substitution in humans, His → Arg (the English mutation), but at His6 rather than His13, may be associated with AD.[18] Whether this mutation is causative or simply a polymorphism remains unclear, but incorporation of this substitution into Aβ has been found to substantially increase β-sheet formation, fibril seeding ability, and formation of toxic oligomers.[19] It thus is reasonable to hypothesize that the presence of the two additional amino acid substitutions in *Mm* Aβ42 explains why wild-type mice do not show AD-like pathology.

It has been suggested that species-specific differences in Aβ42 primary structure are key factors controlling the development of AD-like pathology.[15,20] However, some of the work in this area is contradictory.[16,17,21] Fraser et al.[22] and Hilbich et al.[16] argue that the Arg5Gly, His13Arg, and Tyr10Phe substitutions do not account for the lack of amyloid deposits in the brains of aged rats and mice and have no effect on the morphology and organization of fibrils. In contrast, Ötvös et al.[15] and Dyrks et al.[21] suggest that subtle interspecies differences in amino acid residues *may* account for the inability of the rodent peptide to form amyloid fibrils in situ. Here, we investigate how the natural differences in Aβ protein sequence among humans, *Mm*, and *Od* affect the biophysical, biochemical, and biological properties of the respective Aβ peptides.

RESULTS AND DISCUSSION

Experimental Strategy. We applied a multidisciplinary strategy to elucidate and compare the evolution of secondary, tertiary, and quaternary structure during assembly of human, *Mm*, and *Od* Aβ peptides (for a review, see ref 23). This strategy employs multiple orthogonal approaches to take advantage of the specific revelatory strengths inherent to each. We then examined the neurotoxic activities of the peptide assemblies to establish structure−activity relationships. The ability to cross correlate the results of each experimental approach provides greater insight into system characteristics than does application of each approach in isolation.

Ion mobility−mass spectrometry (IM-MS) coupled with computational modeling allows real time, noninvasive monitoring of peptide tertiary and quaternary structure. It has been very useful in studies of amyloid formation because of its ability to distinguish different conformers and sizes of assemblies in polydisperse and metastable peptide populations, a situation that has complicated the use of other methods.[24] This analysis is done in the gas phase, which has the potential to alter in hydro conformations and assembly states. Comparative studies have suggested that IM-MS results do reflect in hydro assembly states,[25] nevertheless, to ensure the validity of the data thus obtained, we used two additional complementary methods to monitor Aβ assembly, photoinduced cross-linking of unmodified proteins (PICUP), and quasielastic light scattering spectroscopy (QLS).

PICUP is a zero-length photochemical cross-linking method that, when coupled with SDS-PAGE, silver staining, and image analysis, yields the oligomer frequency distribution (for a review, see ref 26). PICUP, like IM-MS, is noninvasive, in that no pre facto modification of Aβ primary structure is involved and no exogenous cross-linking reagents are necessary (the chemistry is radical-based). This technique is particularly suited to study of initial phases of Aβ oligomerization because of its sensitivity and rapidity (ms reaction times). PICUP is less appropriate for studying larger assemblies (monomer number $\gtrsim 20$) because cross-linking efficiency is inversely proportional to monomer number.

QLS measures the diffusion coefficients of particles in solution by determining the time dependence of fluctuations of laser light scattered by them. These coefficients can be converted directly into hydrodynamic radii using the Stokes−Einstein−Sutherland equation,[27,28] providing the means to noninvasively monitor scatterer size in real time. This method has been used extensively for determination of Aβ assembly kinetics, nucleation and elongation rates,[29] and scatterer geometry (for a review, see ref 30). It complements PICUP because its sensitivity depends on the second power of scatterer mass, which means it is especially well suited for monitoring higher-order oligomerization and fibril formation.

Aβ is an intrinsically disordered protein in the monomer state, which means that the methods above are not optimal for revealing conformational fluctuations within that state or as monomer folding and assembly first begins. For this reason, we employ bis-ANS,[31] a dye that fluoresces in low dielectric environments (e.g., when associated with exposed hydrophobic regions of proteins), to interrogate these states. We also use Sypro Orange[32] to control for any effects of bis-ANS on the assembly process itself.[33] We incorporate circular dichroism spectroscopy (CD) to monitor the emanation of regular secondary structure and electron microscopy (EM) to determine, compare, and contrast the morphologies of any assemblies existing immediately following peptide dissolution and after completion of the assembly process (usually the fibril stage).

To establish structure−activity relationships, the structural data acquired using the methods detailed above are correlated with results of three types of neurotoxicity assays performed on early stage assemblies, 3-(4,5-dimethylthiazol-2-yl)-2,5-diphenyltetrazolium bromide (MTT) metabolism,[34] lactate dehydrogenase (LDH) release,[35] and elicitation of apoptosis.

Ion Mobility−Mass Spectrometry (IM-MS) and Aβ42 Monomer Structure. To probe the effects of primary structure difference (Figure 1) on the peptide structure and

DOI: 10.1021/acschemneuro.5b00180
ACS Chem. Neurosci. XXXX, XXX, XXX−XXX

oligomer distributions of all Aβ42 alloforms, we performed an ion mobility coupled mass spectrometry analysis. Ion mobility is capable of separating species that have the same mass-to-charge (m/z) ratio but different conformations or oligomer orders ["order" in this respect refers to the number of monomers per oligomer. Please see ref 25 for a discussion of the relationship between the ratio z/n and oligomer order].[36] It has been successfully applied to the study of Aβ assembly and its inhibition by small molecules.[25,37−45] We first recorded the mass spectra of all three Aβ42 alloforms immediately after preparation (Figure 2a−c). All alloforms displayed three peaks,

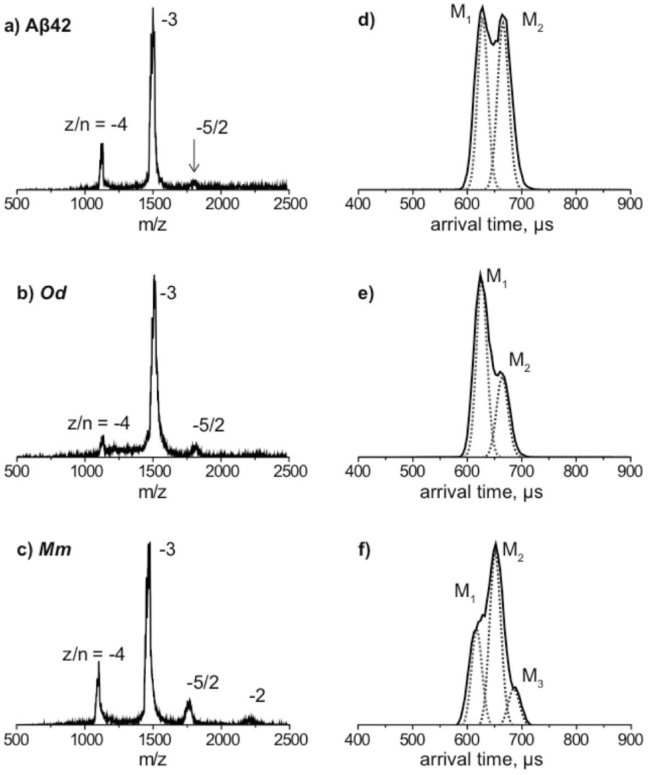

Figure 2. Ion mobility−mass spectrometry and Aβ42 monomer structure. (A−C) Mass spectra of all Aβ42 alloforms. The charge state z/n is noted for each species, where z is the charge and n is the oligomer number. (D−F) The ATDs of z/n = −3 for all Aβ42 alloforms. M_1, M_2, and M_3 represent three monomer conformers with different cross sections.

corresponding to the z/n = −4, −3, and −5/2 charge states, where z is the charge and n is nominal oligomer order. It is notable that the intensity of the z/n = −5/2 peak of *Mm* is relatively high compared to those of Aβ42 or *Od*. These results suggest that *Mm* oligomerizes more readily than do Aβ42 and *Od*. Interestingly, this suggestion is consistent with the observation that *Mm* clogged the nanoelectrospray tips more easily during the experiment than did either Aβ42 or *Od*.

To evaluate peptide monomer structures, arrival time distributions (ATDs) were determined for the z/n = −3 species (Figure 2d−f). In previous studies of the ATD of the z/n = −3 Aβ42 species,[25,37] two major features, with arrival times at ~620 (M_1) and 670 (M_2) μs, were observed. M_1 and M_2 were assigned as a compact solvent free-like conformer and an extended solution-like conformer, respectively. Here, the ATD of the z/n = −3 *Od* also showed two features, which by analogy with the prior samples and analysis of collision cross sections (σ; Supporting Information (SI) Table S1), were assigned as M_1 and M_2. Interestingly, the ATD of the z/n = −3 *Mm* displayed three features, assigned as M_1, M_2, and M_3. M_3 was not observed with the Aβ42 or *Od* peptides. This indicates that *Mm* produces an additional monomer conformer with a more extended structure. As shown in SI Table S1, the collision cross sections of M_1 and M_2 monomers for each peptide were very similar, suggesting that all three Aβ42 alloforms have similar monomer conformations (M_1 and M_2). *Mm* forms one additional extended conformer (M_3), which may be of relevance to its aggregation kinetics.

Ion Mobility Spectrometry and Aβ42 Oligomer Distributions. To understand the initial oligomer distributions of the Aβ42 species, we recorded ATDs of the z/n = −5/2 peaks (Figure 3). The ATD of Aβ42 shows four features, with

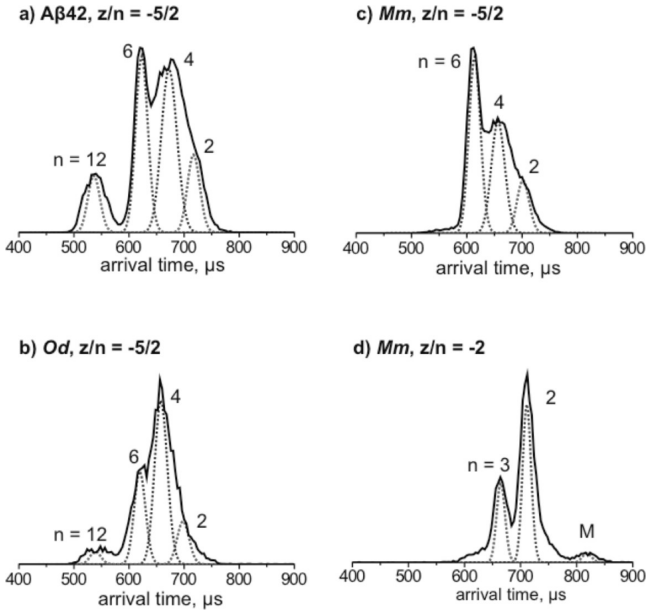

Figure 3. Ion mobility spectrometry and Aβ42 oligomer distributions. (A−C) The ATDs of the z/n = −5/2 peaks for all Aβ42 alloforms. (D) The ATD of the z/n = −2 peak for mouse Aβ42. The oligomer number (n) is noted for each feature.

arrival times at ≈ 710, 680, 620, and 540 μs. These features were assigned as dimer, tetramer, hexamer, and dodecamer based on their collision cross sections (SI Table S1; see also Bernstein et al.[38] for a detailed discussion of Aβ42 oligomer assignments). The ATD of *Od* also shows these four features. However, the ATD of *Mm* shows only three features, corresponding to dimer, tetramer, and hexamer. Finally, the ATD of the z/n = −2 *Mm* was recorded and showed predominant features, corresponding to dimer and trimer (Figure 3d), indicating that *Mm* formed trimer, something not observed for Aβ42 or *Od* under the same experimental conditions. The lack of dodecamer formation by *Mm* is interesting, as it may correlate with the fact that *Mm* does not naturally display AD-like neuropathology, in contrast to mice expressing the human form of Aβ,[46] which express substantial levels of A$\beta^\star$56, a dodecamer linked to memory deficits.

Oligomerization of Aβ42 by PICUP. We next performed photochemical cross-linking of unmodified proteins (PICUP) and SDS-PAGE (Figure 4), an approach that "freezes" the monomer ⇌ oligomer equilibrium, thus allowing quantitative determination of Aβ42 oligomer size distributions.[26] As

DOI: 10.1021/acschemneuro.5b00180
ACS Chem. Neurosci. XXXX, XXX, XXX−XXX

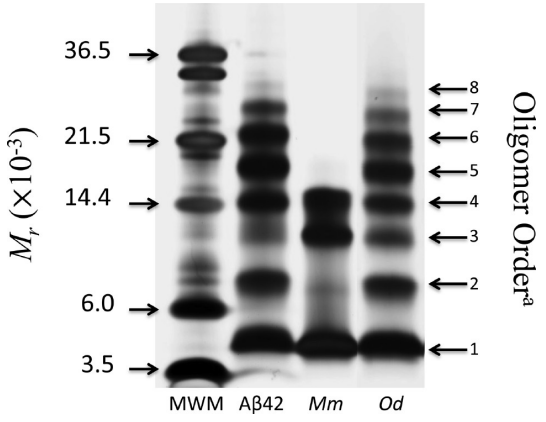

Figure 4. Oligomer distributions determined by PICUP. PICUP, followed by SDS-PAGE and silver staining, was done to determine the oligomer size distributions of the peptides. (a) Oligomer order arrows point to positions of bands from the Aβ42 lane. Some variation in electrophoretic mobility is observed among the other peptides.

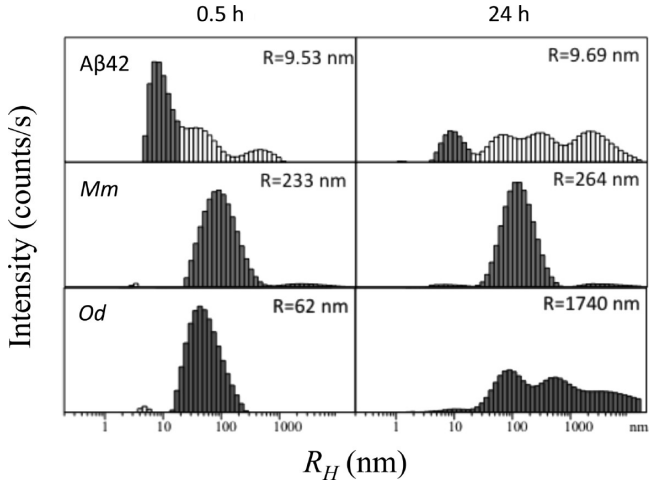

Figure 5. Quasielastic light scattering spectroscopy (QLS). Distribution of the intensity (counts/second) of light scattered by particles of various hydrodynamic radii present in solution. The data are from samples monitored ≈30 min after sample preparation (left panels) and after 24 h (right panels). The number in the top right corner of the panel represents the average R_H for the shaded regions of the distributions. Buffer spectra produce no scattering and thus are not shown.

discussed above, PICUP complements, and is orthogonal to, IM-MS. Aβ42 displayed a typical PICUP wild-type Aβ42 oligomer distribution (see ref 47) comprising a series of oligomers with a prominent node of band intensity at pentamer−hexamer. *Mm* showed a relatively faint dimer but intense trimer and tetramer bands. With the exception of the faint dimer band, this oligomerization pattern is identical to that of non-cross-linked Aβ42 (SI Figure S1), which we would expect due to the fact that the Tyr10Phe amino acid substitution in the *Mm* peptide eliminates the Tyr residue that is highly reactive in the PICUP chemistry. The intense trimer and tetramer bands also were present in the non-cross-linked control *Mm* sample (SI Figure S1), again consistent with a lack of cross-linking of *Mm*. [We note that the trimer and tetramer bands present in cross-linked samples *do* comprise covalently linked oligomers, as determined by repeated excision and re-electrophoresis of these bands (Hayden et al., manuscript in preparation). The bands "run true".] The *Od* PICUP results, on the other hand, are highly similar to that of Aβ42. The His13Arg substitution thus did not appear to alter peptide oligomerization, as measured by PICUP. These results are consistent with the ion mobility results in that *Mm* forms smaller oligomers than do Aβ42 or *Od*.

Monitoring Aβ Assembly by Quasielastic Light Scattering Spectroscopy (QLS). To monitor rates of peptide assembly, as well as to provide a third, noninvasive, orthogonal method for determining assembly sizes, we employed QLS. This method provides diffusion coefficients (D) of particles in solution.[48] We used QLS, and the Stokes−Einstein−Sutherland equation (see Methods), to derive R_H distributions of each peptide after 0.5 and 24 h of incubation (Figure 5). Aβ42 initially produced a distribution composed primarily of small particles of $R_H \approx 8-10$ nm (darkened area). Particles of $R_H \sim 100-1000$ nm also were observed, but because scattering intensity is proportional to the square of molecular weight, these peaks must have been produced by relatively few particles. After 24 h, the contributions to the scattered light intensity of larger particles had increased substantially, consistent with a process of Aβ assembly. However, oligomers of $R_H \approx 8-10$ nm remained. [The scattering intensity varies as the square of the molecular weight of the scatterer. The maximum intensity of small scatterers (shaded bars) was equivalent to those for larger scatterers (unshaded bars), which means that a disproportionate percentage of scatterers in this mixture were small. For the purpose of comparison between the two time points, we focused on these small scatterers when we calculated scatterer R_H.] Such oligomers have been reported previously.[49] In contrast, the other peptides did not form oligomers of this size. After 24 h of incubation, the distribution of *Mm* changed little, showing only a slightly increased average R_H of its predominant peak. Deconvolution of R_H distributions depends on the specific parametrizations used, especially that for data smoothing.[48] Although deconvolution yielded two peaks for *Mm*, it is possible that only one heterodisperse population of scatterers was present. For this reason, the average R_H was calculated across the entire distribution. We applied the same approach to calculate the average R_H of *Od*, the data from which produced three apparent nodes of R_H intensity following smoothing, at ≈90, ≈500, and ≈4000 nm. The average R_H of this distribution was 1740 nm, indicating the presence of much larger assemblies than observed at the same time in the other samples.

Interestingly, the time-dependence of the distributions of R_H showed that those of Aβ42 and *Od* primarily comprised relatively small scatterers initially ($\overline{R_H} \approx 10$ nm and $\overline{R_H} \approx 62$ nm, respectively) but that after 24 h the distribution range expanded to larger sizes with maximal $R_H > 1000$ nm. *Mm* was unique in initially displaying larger scatterers ($\overline{R_H} \approx 233$ nm) whose size remained relatively constant over 24 h.

It should be noted that all samples were filtered through a 20 nm porosity filter immediately after preparation. During the first 30 min of monitoring, for all peptides except Aβ42, we observed a rapid increase in scatterer size, reflecting a rapid assembly process. The particle size distributions then were relatively stable while overall scattering intensity continued to rise due to increasing contribution to scattering from large particles. We calculated the *relative* rate of growth, $(dI/dt)/I_0$, in the scattering intensity during the first hour of incubation, where I is intensity, t is time, and I_0 is initial intensity (see

DOI: 10.1021/acschemneuro.5b00180
ACS Chem. Neurosci. XXXX, XXX, XXX−XXX

Table 1). Rates for Aβ42 and *Mm* were moderate, consistent with relative constancy of their particle size distributions. In contrast, *Od* displayed a much higher rate, as would be expected from the relatively large scatterer size observed after incubation for 24 h (Figure 5).

Table 1. Rate of Change in Scattering Intensity[a]

peptide	$(dI/dt)/I_0$
Aβ42	0.05
Mm	0.09
Od	1.43

[a]The rate of change in scattering intensity, dI/dt, determined by fitting I_t to a linear function spanning the first hour of incubation. I_0 was determined from the derived line $I_t = dI/dt \times t + I_0$ by substitution of $t = 0$. Both dI/dt and I_0 depend on the aperture in which light is collected, which in turn is a function of the instrument used. To determine the instrument-independent rate of change in relative intensity, we report the normalized quantity $(dI/dt)/I_0$. We note that these quantities are precise, but likely not absolutely accurate, because the intensity versus time dependency over this time interval is significantly nonlinear.

It should be noted that while the quantity $(dI/dt)/I_0$ is instrument independent and precise, it is greatly affected by the initial aggregation state of the sample immediately after filtration and before the first measurement can be taken. As seen in Figure 5, in the Aβ sample at 0.5 h, little aggregation had yet occurred. Most particles were still of the sizes that passed through the 20 nm filter and therefore the quantity $(dI/dt)/I_0$ in Table 1 reflects the actual initial relative growth rate of the *Z*-averaged mass of these scatterers. In contrast, in the *Mm* sample, aggregation occurred very rapidly after filtration, with particles reaching sizes >200 nm before the first measurements could be completed. As a result, the initial value of I_0 is large and the small value of $(dI/dt)/I_0$ reflects the fact that no significant increase in the mass of the scatterers occurs after the very fast initial aggregation of the peptide. In *Od*, aggregation occurred much faster than in Aβ, but much slower than in *Mm*, and was observed during the first hour of incubation. Had fast aggregation increased I_0 in this sample immediately after filtration, the value of $(dI/dt)/I_0$ of 1.43 would have been an underestimation of the actual relative growth rate of the *Z*-averaged mass of the scatterers. In summary, the values in Table 1 reflect the actual initial aggregation rate of Aβ, the actual, or slightly underestimated initial rate of aggregation of *Od*, and the late stage aggregation rate of *Mm* (because its early stage aggregation cannot be monitored in the time necessary to prepare the sample and place it into the QLS instrument).

Taken together, the data on the time-dependent evolution of R_H and scattering intensity suggest that *Mm* rapidly forms small aggregates that are relatively stable, whereas both Aβ and *Od* display a lag time before frank fibril assembly is observed.

Bis-ANS Fluorescence. We monitored exposure of hydrophobic surfaces during peptide assembly using Bis-ANS fluorescence (Figure 6). Bis-ANS is a hydrophobic molecular probe that is essentially nonfluorescent in water but fluorescent in nonpolar or hydrophobic environments. This property makes it a sensitive indicator of protein conformation (e.g., molten globules, exposed hydrophobic surfaces, or native folds).[32,50−53]

Aβ42 showed a rapid but modest increase in fluorescence during the first 4 h of incubation (to ≈200 FU), after which a slow monotonic decrease in fluorescence was observed. *Mm*

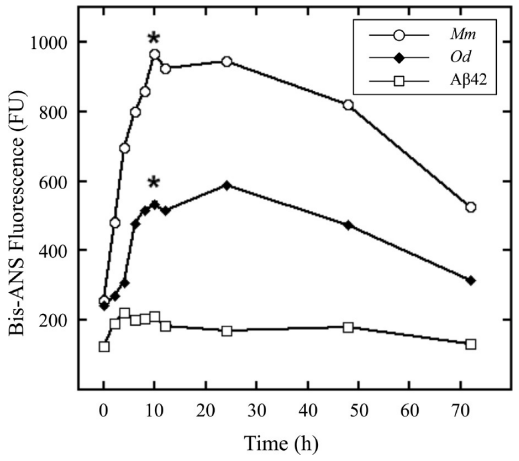

Figure 6. Bis-ANS fluorescence. Aliquots from Aβ assembly reactions were removed at regular intervals, mixed with Bis-ANS, and then monitored for fluorescence (as arbitrary fluorescence units (FU)). Asterisks indicate statistically significant ($p < 0.05$) differences relative to Aβ42.

displayed an initial level of fluorescence approximately twice that of Aβ42 that eventually reached ≈950 FU, the highest among these peptides. Fluorescence then decreased monotonically with time. *Od* displayed initial fluorescence levels identical, within experimental error, to that of *Mm*. The peak level of *Od* fluorescence was ∼600 FU, which occurred at ≈24 h, later than for Aβ42 or *Mm*. Experiments also were done with SYPRO Orange (data not shown), a dye with properties similar to that of Bis-ANS. The rates of fluorescence increase and the plateau levels of fluorescence produced by SYPRO Orange exhibited the same rank order as with Bis-ANS, namely *Mm* > *Od* > Aβ42.

The rapid increase in fluorescence in the *Mm* sample suggests early exposure of hydrophobic surfaces. The formation of such surfaces has been postulated to occur as the intrinsically disordered Aβ monomer begins folding.[54,55]

Secondary Structure Dynamics. We used circular dichroism spectroscopy (CD) to determine the time-dependence of the distribution of secondary structures for each peptide (SI Figure S2). Assignment of secondary structures was done by inspection based on comparison to α-helix, β-sheet, and statistical coil basis spectra.[56,57] Aβ42 displayed statistical coil structure initially, but then exhibited a progressive increase in β-sheet content that was clear within hours and produced a classical β-sheet spectrum at 24 h. The spectra appeared to display an isodichroic point at ≈208 nm. This isodichroic point was observed with all three peptides, suggesting the existence of a two-state transition (likely statistical coil → α-helix).[58] *Mm* exhibited *some* β-sheet content immediately after preparation. Progressive increases in β-sheet were observed throughout the 24 h monitoring period, as with Aβ42. However, the level of β-sheet was higher than in Aβ42, as indicated by the relative increase in absolute values of the molar ellipticities at ≈195 and ≈215 nm. *Od* had the least statistical coil content of any of the peptides when its CD spectrum was first acquired. Its initial β-sheet content was similar to that of *Mm*, and β-sheet content displayed a progressive increase with a rate similar that of Aβ42.

As peptide folding and assembly occur, a minimum of $[\Theta]_\lambda$ appears in the region 215−218 nm (Figure 7). We infer from the position of this minimum and the shapes of the cognate curves that the minimum reflects β-sheet content. *Mm* showed

DOI: 10.1021/acschemneuro.5b00180
ACS Chem. Neurosci. XXXX, XXX, XXX−XXX

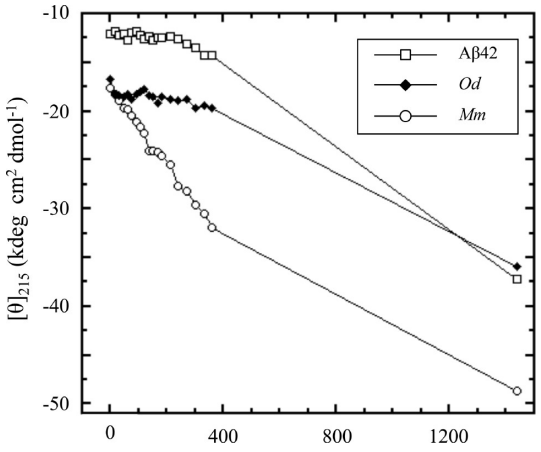

Figure 7. Time-dependence of $[\Theta]_{215}$. Molar ellipticity at 215 nm is plotted versus time as a measure of time-dependent changes in β-sheet secondary structure.

the highest initial β-sheet content (the most negative $[\Theta]_{215}$), the fastest increase in the level of this secondary structure element (largest $|d[\Theta]_{215}/dt|$), and the highest overall β-sheet content at the end of the experiment (the most negative $[\Theta]_{215}$). *Od* also displayed relatively high initial β-sheet content, but the evolution of β-sheet occurred at a slower rate. Aβ42 had the lowest initial β-sheet level, but this level eventually reached that of *Od*. The high initial β-sheet in the *Mm* peptide is consistent with its rapid oligomerization. The monotonic increase in β-sheet for all three peptides suggests a progressive assembly phenomenon that was confirmed in subsequent EM experiments (see below).

Assembly Morphology. We used EM to determine the morphologies of the assemblies formed by the three peptides (Figure 8). To do so, we compared morphologies at the beginning (0.5 h) of the assembly process and when the process was completed (7 d). Insight into the kinetics of assembly provided by the experiments discussed above suggested that these time points were appropriate for our purpose. Small structures ("globules") were observed initially in the Aβ42 sample. These globules ranged in diameter from 11 to 23 nm (white arrows, Figure 8), often displaying pore-like central cavities filled with uranyl acetate stain. These annuli had outside diameters ranging from ≈13 to 25 nm and inside diameters ranging from ≈4 to 11 nm. *Mm*, in contrast, formed aggregates comprising short beaded chains of different diameters (black arrows) and irregular structures (open arrows). These irregular assemblies ranged in diameter from 11 to 21 nm and had lengths from 16 to 75 nm. *Od* displayed filamentous aggregates (open arrows), as well as occasional long filaments to which smaller assemblies appeared to be associated (curved arrow). Small globules (black arrows) were interspersed among these other structures. The globules range in diameter from 11 to 54 nm. The diameters of the long fibrils ranged from ≈7 to 19 nm.

Considering the heterogeneity of assembly morphologies observed immediately after sample preparation, it was interesting that by 7 days all samples formed long straight or

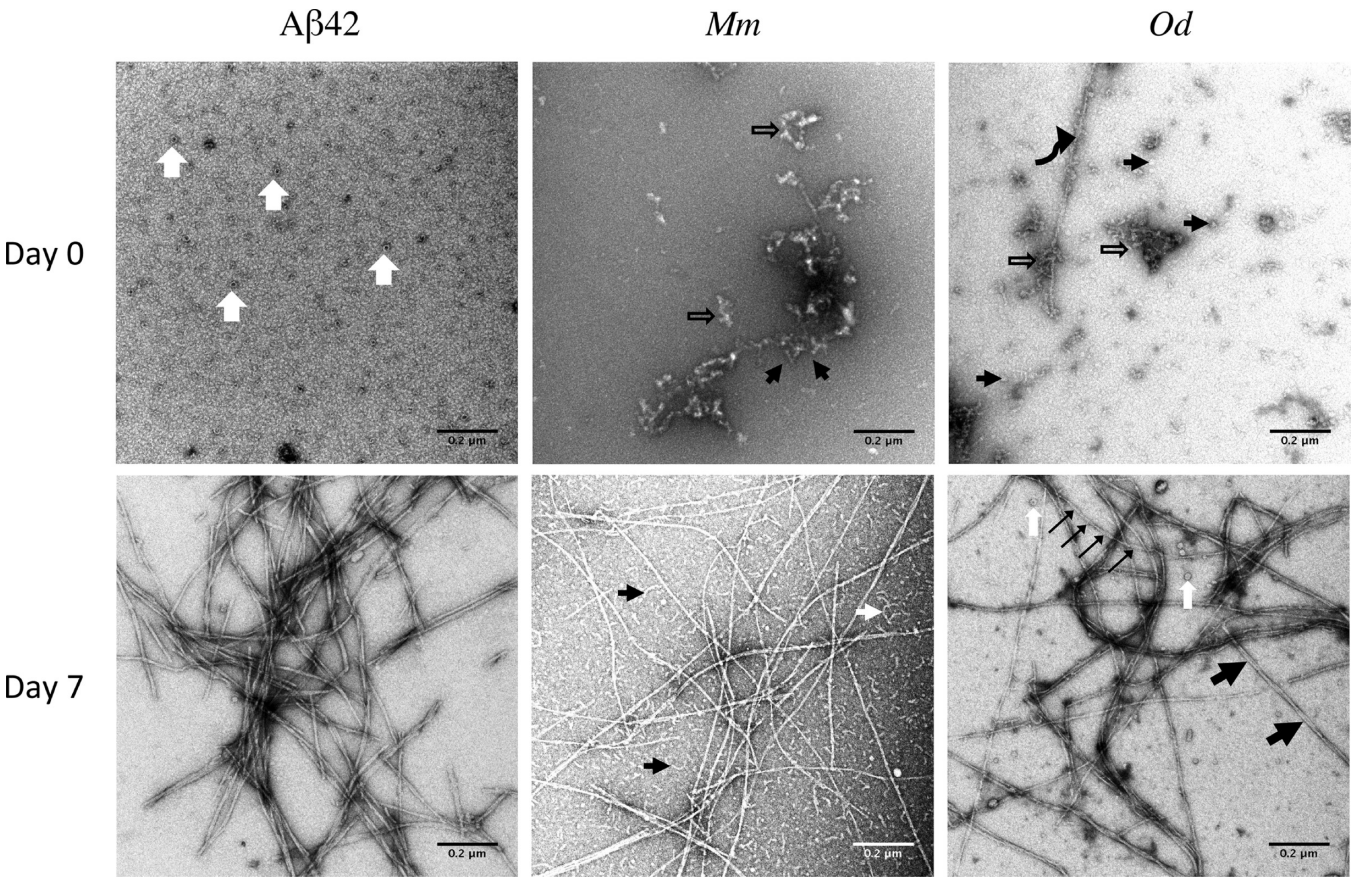

Figure 8. Assembly morphology. EM was used to determine assembly morphology. Aliquots of assembly reactions were removed at days 0 and 7. Determination of geometric parameters (lengths, diameters) was done using Image-J software. Scale bars are 200 nm.

DOI: 10.1021/acschemneuro.5b00180
ACS Chem. Neurosci. XXXX, XXX, XXX−XXX

Table 2. Dimensions of Assemblies Observed by EM[a]

	day 0			day 7		
peptide	globules	short fibrils	long fibrils	globules	short fibrils	long fibrils
Aβ42	11−23				7−12 (56−303)	9−21
Mm	11−21 (16−75)					4−19
Od	11−54		7−19	7−17	7−17 (37−182)	7−17

[a]Peptides were incubated at 37°C with shaking. Aliquots of assemblies were removed at day 0 and day 7. Following incubation, different classes of assemblies were observed, including globules, short fibrils, and long fibrils. If present, the numbers in parentheses represent the size range, in units of nm, of each assembly type. Assembly lengths are reported in nm within parentheses.

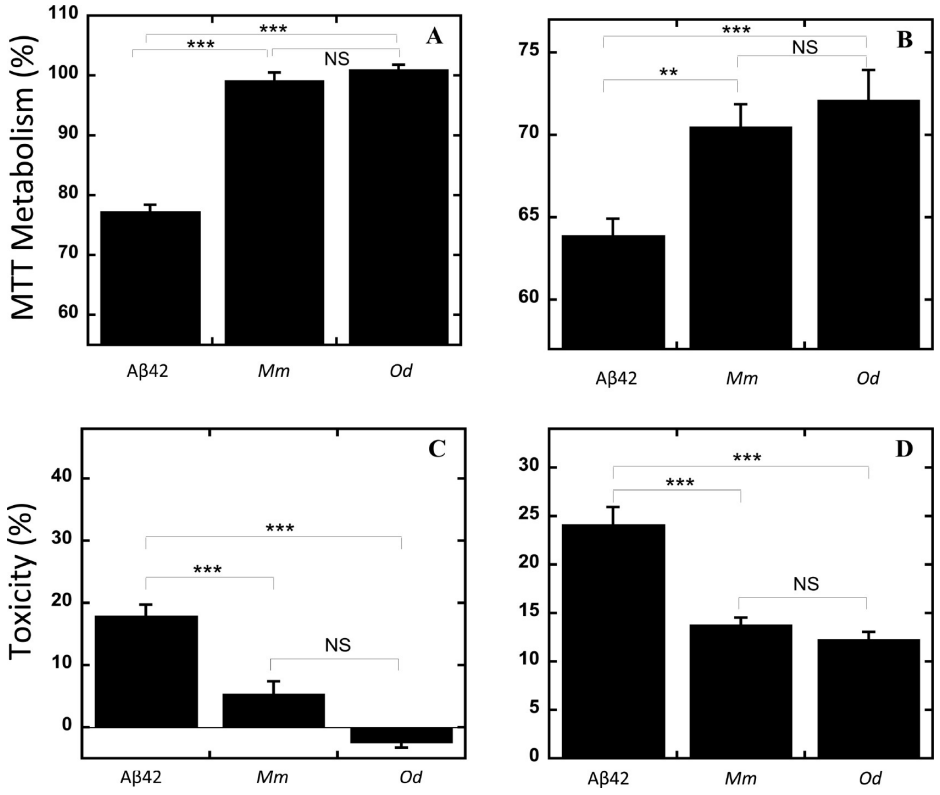

Figure 9. Peptide neurotoxicity. To determine the effects of the different peptides on cellular metabolism, MTT assays were performed using (A) differentiated PC12 cells or (B) rat primary cortical neurons. Freshly prepared peptides were added to the cultures for 24 h at 37 °C, after which MTT was added and incubated for 4 h at 37 °C, stop solution was added to the cultures, the cultures were incubated overnight, and then reference corrected formazan optical absorbance was measured (see Methods). Data are representative of that obtained in three independent experiments (six wells per data point). The data are normalized to the media control group and expressed as mean ± the standard error of the mean (SEM). Statistical significance between samples is indicated by asterisks (*** and ** indicate p values <0.001 and <0.01, respectively). NS is "not significant." To determine membrane integrity, LDH activity was measured in the media from (C) differentiated PC12 cells or (D) rat primary cortical neurons after 48 h of incubation of the cells with the different peptides. Data are representative of that obtained in three independent experiments (six wells per data point). The data are normalized to the media control group and expressed as mean toxicity ± the standard error of the mean (SEM). Statistical significance between samples is indicated by asterisks (*** and ** indicate p values <0.001 and <0.01 respectively). NS is "not significant".

curved fibrils. Aβ42 predominately formed fibrils of quite different lengths (56−303 nm) and with diameters of ≈7−12 nm (Table 2). Long fibrils had a diameter of 9−21 nm. The *Mm* sample contained numerous fibrils that were thinner than those of Aβ42 (Table 2) but also abundant smaller curved "protofibril-like" structures (black and white arrows).[59] *Od* formed long and short fibrils interspersed with numerous globules. Bifilar structures with helical twist were observed (thick black arrow) along with thinner fibrils, often with helical twists (thin black arrows). A number of annuli also were observed (white arrows). The results of electron microscopic examination of assembly morphology correlated with the results from the prior experiments. For example, the initial rank order of average assembly size was *Mm* > *Od* > Aβ42, and as would be predicted from the QLS and CD experiments, large (fibrillar) assemblies were observed after 7 d. *Mm* continued to behave somewhat uniquely in that the distribution of assemblies at day 7 included abundant protofibrillar species (not seen with the other peptides) and narrower fibrils. The continued presence of the small protofibrils is consistent with the relatively constant distribution of scatter sizes seen during the first 24 h by QLS.

Neurotoxic Activities of Aβ Assemblies. MTT assays were performed to evaluate the effects of freshly prepared peptides on MTT metabolism.[60] The assay was performed both on PC12 cells (Figure 9A) and rat primary cortical neurons (Figure 9B). Aβ42 caused an ≈23% decrease in MTT metabolism in PC12 cells, whereas *Mm* and *Od* were nontoxic.

DOI: 10.1021/acschemneuro.5b00180
ACS Chem. Neurosci. XXXX, XXX, XXX−XXX

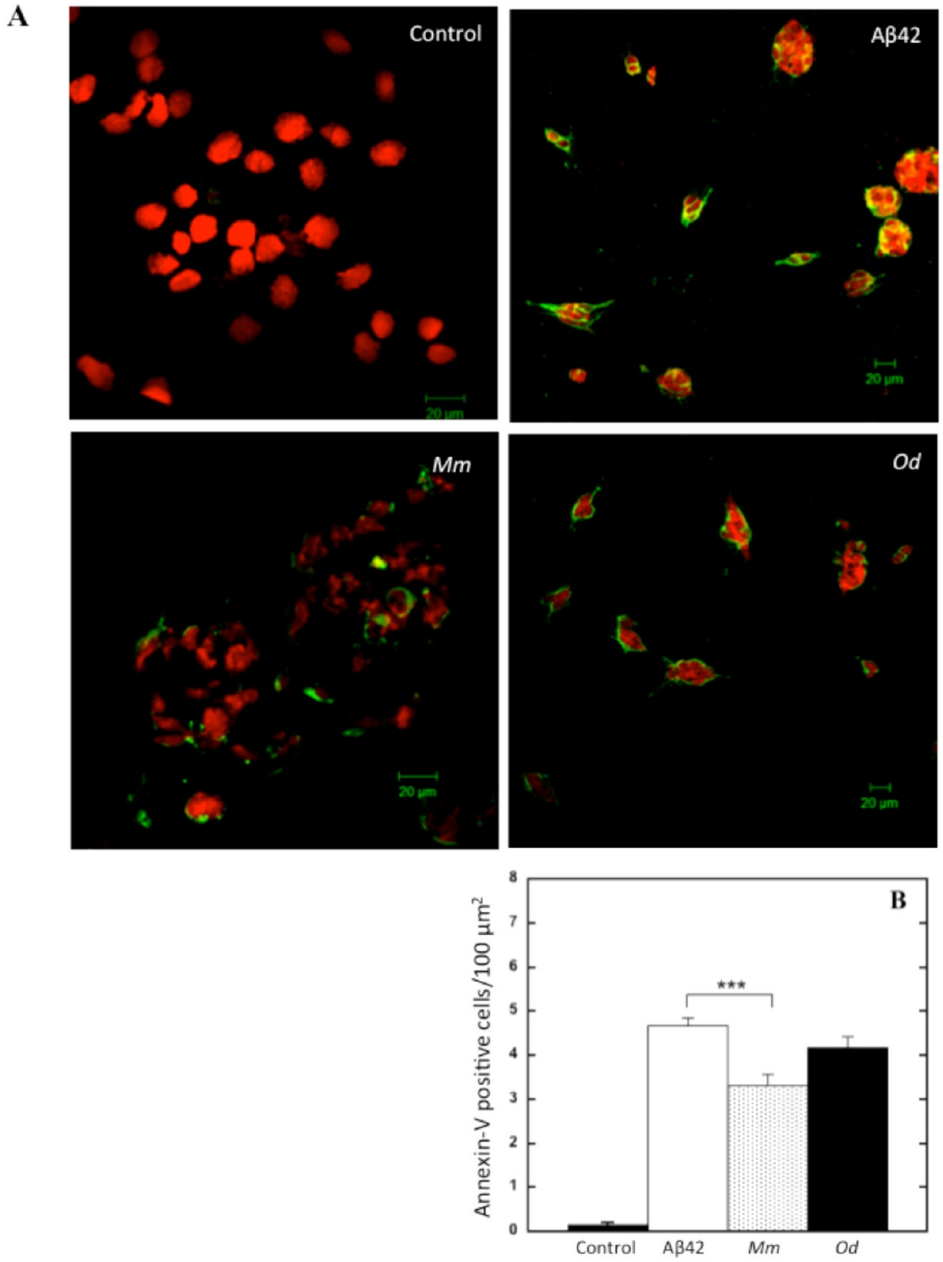

Figure 10. Monitoring apoptosis. (A) Annexin V staining of SH-SY5Y cells treated with each of the peptides was performed to estimate apoptosis levels. The SH-SY5Y cells were grown on coverslips and treated with freshly prepared Aβ42 peptides for 24 h, after which they were stained with Annexin V-FITC. Images were recorded using confocal laser scanning microscopy. (B) Bar graph: quantitation of Annexin V staining. The number of apoptotic cells was counted in a 100 μm^2 area using Image-J software. A minimum of 30 microscopic fields was used in each of two independent experiments. Significance between groups is indicated by asterisks (*** and ** indicate p values of <0.001 and <0.01, respectively). No significant difference existed between *Mm* and *Od*, although it is possible that *Od* trended toward greater apoptotic activity.

The differences in toxicity between Aβ42 and each of the other peptides were highly significant ($p < 0.001$). The data from primary cortical neurons were similar to those from PC12 cells. Quantitatively, the levels of toxicity of all peptides assayed with primary cortical neurons were greater than with PC12 cells. LDH release assays were performed to measure membrane integrity. The results of these assays were consistent with those of the MTT assays (Figure 9C,D). Aβ42 caused the most release of LDH whereas *Mm* and *Od* caused the least release.

To measure the level of apoptosis induced by freshly prepared Aβ, SHSY-5Y cells were stained for phosphatidylserine using Annexin V-conjugated FITC.[61,62] Propidium iodide (PI) staining was done concurrently to reveal cell nuclei. Negative control samples displayed only red nuclei, but no cell surface Annexin V fluorescence. Positive control samples incubated with 1 μM staurosporine, showed complete disruption of membrane integrity (data not shown). All peptides produced green fluorescence, indicating binding of Annexin V (Figure 10). Quantitative analysis of the number of Annexin V-positive (fluorescent) cells per 100 μm^2 field (Figure 10B, bar graph) revealed an average of 4.7 for Aβ42 and 4.2 for *Od*, a difference that was not statistically significant. *Mm* showed significantly lower numbers (3.3; $p < 0.01$) than did Aβ42. The difference in fluorescence between *Od* and *Mm* was not significant.

DOI: 10.1021/acschemneuro.5b00180
ACS Chem. Neurosci. XXXX, XXX, XXX−XXX

Table 3. Summary of Experimental Results[a]

peptide	MS (z/n)	ATD (n)	PICUP (n)	R_H (nm)	$(dI/dt)/I_0$ (h^{-1})	bis-ANS (FU)	ThT (FU)	EM (nm)	MTT (%)	LDH (%)	apoptosis (no.)
Aβ42	−4, −3, −5/2	2, 4, 6, 12	5−6	8−10	0.05	+	+	9−21	++	++	+++++
Mm	−4, −3*, −5/2	2, 3, 4, 6	3, 4	233	0.09	+++++	++++	4−19	−	−	+++
Od	−4, −3, −5/2	2, 4, 6, 12	5−6	62	1.43	+++	++	7−17	−	−	++++

[a]The symbol + signifies an effect. Increased effect is indicated by increased numbers of + signs. Columns are peptide, the peptide to which the results in each line refer; MS, predominant peaks in MS according to their charge/oligomer order ratios (z/n) (−3* for *Mm* signifies this peak intensity was substantially larger with *Mm* than with the other two peptides); ATD, oligomer orders inferred from arrival time distributions of z/n = −5/2 and −2 ions, determined immediately after peptide dissolution; PICUP, n refers to the predominant oligomer order(s) observed in PICUP experiments; R_H, hydrodynamic radius (nm) observed using QLS 30 min after peptide dissolution; $(dI/dt)/I_0$, rate (h^{-1}) of increase in scattering intensity (dI/dt) normalized to the initial scattering intensity (I_0) of each peptide; bis-ANS, hydrophobic surface exposure assayed using bis-ANS fluorescence (FU are arbitrary fluorescence units); ThT, β-sheet content assayed at the end of the assembly process using ThT fluorescence intensity (FU are arbitrary fluorescence units); EM, diameter (nm) range of fibrils; MTT, ability of peptide to interfere with MTT metabolism in differentiated PC12 cells; LDH, ability of peptide to disrupt membrane integrity of differentiated PC12 cells, as measured by LDH activity; apoptosis, annexin-V-positive cells/100 μm^2 (the numbers were 4.7, 3.3, and 4.2, for Aβ42, *Mm*, and *Od*, respectively, and only *Mm* produced a number significantly ($p < 0.01$) different that of Aβ42).

Taken together, the results among these assays were consistent and showed a rank order of toxicity of Aβ42 ≫ *Mm* ∼ *Od*. An identical rank order was observed in our Annexin V fluorescence apoptosis assay. This rank order was the opposite of the rank order observed in our biophysical studies. Considered from the perspective of assembly rate (which is inversely related to assembly size) versus toxicity, our data suggest that assembly populations comprising smaller assemblies are relatively more toxic than are those containing larger assemblies. This result agrees with the hypothesis that the most important neurotoxins in AD are small, presumably oligomeric, assemblies.[63−65] However, our data extend this hypothesis by providing evidence, through the use of peptides from different species (and of different primary structure), that assembly state, rather than primary structure per se, is likely to contribute most significantly to peptide neurotoxicity.

SUMMARY

We have discussed in detail above the results of our studies, which we summarize in Table 3. One of the most interesting insights this table provides into the three peptides examined is the apparent uniqueness of *Mm*. This peptide has an exceptionally high propensity to form trimers, as ascertained by MS, ATD, and PICUP, whereas trimers are not the predominant species observed with Aβ42 or *Od*. ATDs show the presence of dodecamers of Aβ42 and *Od* but none of *Mm*. A particularly interesting feature of the ATD of *Mm* is the presence of a monomer conformer, M3, that is not formed by the other peptides and has the most extended shape of any of the three monomer states (i.e., M1−M3). This conformation is consistent with, and may explain, the finding that bis-ANS fluorescence was substantially higher with *Mm* than with Aβ42 or *Od*. Initial exposure of hydrophobic surface could facilitate oligomerization into trimers structurally organized in a manner facilitating rapid assembly. This suggestion is consistent with QLS data showing that *Mm* assembled exceptionally rapidly (before the first QLS measurement could be made) to form large scatterers (R_H = 233 nm) and why its subsequent normalized assembly growth rate ($(dI/dt)/I_0$) was low. Rapid aggregation into fibrils explains the especially robust ThT binding shown by *Mm*. It may also explain the lack of, or relatively modest, effects of *Mm* assemblies on MTT metabolism, LDH release, and apoptosis. The potent toxicity of Aβ42 likely represents the converse behavior, namely that the relatively small size of its initial assemblies (8−10 nm), the lack of exposure of hydrophobic surface (bis-ANS = +), slow growth in scatterer size ($(dI/dt)/I_0$ = 0.05), and very modest ThT binding resulted in the emanation of substantial numbers of oligomeric assemblies that were more toxic (MTT and LDH of ++ and apoptosis of +++++) than were the end-stage fibrils. *Od* displayed early oligomerization characteristics similar to those of Aβ42 (MS, ATD, PICUP) but substantially faster normalized growth in size ($(dI/dt)/I_0$ = 1.43) relative to Aβ42 and *Mm*, likely because its hydrophobic surface exposure was greater than Aβ42 and its initial assembly state was much smaller than that of *Mm*. Formation of large assemblies, leading to a relative paucity of lower-order assemblies, may again explain the low toxicity of *Od* in MTT and LDH experiments. The same inverse relationship between assembly size and toxicity appears to operate with respect to apoptosis.

CONCLUSIONS

We suggest that it is the combination of at least three factors that control peptide neurotoxicity: (1) primary structure, (2) assembly structure, and (3) non-Aβ factors. Primary structure determines the intrinsic propensity of a peptide sequence to fold into an energetically determined distribution of tertiary structures, according to Anfinsen.[66] It is the basis of assembly structure, which encompasses the vast and complex folding landscape of Aβ and other amyloid proteins[67] that includes assemblies such as oligomers (irregular, globular, annular, worm-like), protofibrils, and fibrils. In the absence of post-translational modification, primary structure is intrinsic to the Aβ peptide per se and to its folding propensities. However, "non-Aβ factors" may play equally or more important roles with respect to toxicity. Folding pathway choice, which determines whether toxic assemblies form, can be affected by local environmental factors, including pH,[68,69] solvent composition,[70] metals,[71] molecular crowding,[72] membranes and membrane components,[73−75] and protein chaperones.[76] An excellent example of "organismal control" of amyloid protein assembly comes from recent studies of superoxide dismutase 1 (SOD1) aggregation in transgenic mouse models of amyotrophic lateral sclerosis. Bergh et al.[65] report that SOD1 aggregates formed in the brains and spinal cords of these animals differ in structure from those produced in vitro, a clear example of how organismal factors mediate the intrinsic assembly propensities of amyloid proteins and thus may affect their neurotoxic activities. Cellular processes controlling Aβ metabolism, especially those involving Aβ production and

DOI: 10.1021/acschemneuro.5b00180
ACS Chem. Neurosci. XXXX, XXX, XXX−XXX

elimination, determine the biological half-lives of toxic assemblies and thus may be important in mediating Aβ neuropathology.[77−81]

Another potential species-specific non-Aβ factor accounting for the lack of AD-like neuropathology in rodents is sequence differences between human and rodent APP[82,83] outside of the Aβ-coding region. If such differences in APP affected expression levels, then overexpression of the mouse gene might cause neuropathology. However, this does not appear to be the case.[84] Sequence differences between human and rodent PS1 and PS2 also exist.[85] Expression of normal human PS1 or PS2 in transgenic mice does not appear to cause neuropathology, although it does produce an increase in Aβ peptide levels and some behavioral impairment (for a review, see ref 86). Profound effects on Aβ-induced neuropathology have been observed in transgenic mice coexpressing human APP and PS1 proteins linked to familial AD.[87] These results suggest that species-specific sequence differences in PS, or in APP outside of the Aβ coding region, are not the primary explanation for the lack of neuropathology in wild-type rodents.

Taken together, these data do *not* support long-standing hypotheses that the primary factor controlling development of AD-like neuropathology in rodents is Aβ sequence. If it were, then we would *not* expect, *a priori*, to observe the folding and assembly of rodent peptides into intrinsically toxic oligomeric, protofibrillar, and fibrillar structures. Instead, our data support the hypothesis that the factors of *assembly quaternary structure* and *organismal response* control development of neuropathology. The implication of this hypothesis is that a valid understanding of disease causation within a given system (organism, tissue, etc.) requires the coevaluation of both biophysical and physiologic properties of that system. One obvious property that might contribute to amyloid formation is life span. AD amyloidosis in humans is a neuropathologic phenomenon that is age-dependent. Rats of the species *O. degus*, like the naked mole rat, live substantially longer than do animals of the species *M. musculus* (≈6−8 in captivity versus ≈2 years) and thus they may be more likely to develop amyloid and experience its attendant effects. Another interesting possibility, although one beyond the scope of study at this time, is that *O. degus* neurons are more susceptible to Aβ-induced toxicity.

METHODS

Chemicals and Reagents. All chemicals were purchased from Sigma Chemical Co. (Saint Louis, MO) and were of the highest purity available. Water was deionized and filtered using a Milli-Q system (Millipore Corp., Bedford, MA). Xpress silver-staining kits were from Invitrogen (Carlsbad, CA). Buffers were prepared with sterile, autoclaved water containing 0.002% (w/v) sodium azide. SYPRO Orange dye was purchased from Invitrogen Corp. Annexin V staining kits were purchased from BioVision, Inc., Milpitas, CA.

Peptide Synthesis and Preparation. Aβ42 peptides were synthesized using 9-fluorenylmethoxycarbonyl (Fmoc) chemistry and purified by reverse phase high performance liquid chromatography (RP-HPLC), essentially as described.[59] The identity and purity (usually >97%) of the peptides were confirmed by amino acid analysis, mass spectrometry, and reverse phase high performance liquid chromatography (RP-HPLC). Peptides were solvated with 1,1,1,3,3,3-hexafluoroisopropanol (HFIP) as described.[88] Briefly, 100−300 μg of peptide lyophilizate were dissolved in 200 μL of 100% HFIP in a 1.5 mL V-bottom polypropylene microcentrifuge tube (Eppendorf, Fisher Scientific). Each tube was covered with a Kimwipe (Fisher Scientific) tissue and placed in a chemical fume hood overnight to allow evaporation of the HFIP. Tubes then were placed in a SpeedVac rotary evaporator (Savant SPD121P, ThermoScientific) for 2 h to ensure complete HFIP removal. The resulting peptide films were dissolved in 10% (v/v) 60 mM NaOH, 45% (v/v) Milli Q water, followed by 45% (v/v) phosphate buffer (20 mM sodium phosphate, pH 7.5, containing 0.002% (w/v) sodium azide). The solutions then were thoroughly mixed and sonicated for 1 min in a Branson 1200 bath sonicator (Branson Ultrasonics Corp., Danbury, CT). The resulting peptide solution either was used immediately or stored at −20 °C for future use. When used immediately, the sample was placed on ice and the peptide concentrations were estimated by UV absorbance using ε_{280} = 1280 cm^{-1} M^{-1} (for human and *Od*, which contain a Tyr residue) and ε_{257} = 200 cm^{-1} M^{-1} (for *Mm*, which only contains Phe). The final concentration of Aβ42, as necessary for each experiment, was achieved by dilution with phosphate buffer. Equimolar amounts of Aβ42 were used in each experiment and a minimum of three independent experiments was performed.

Ion Mobility−Mass Spectrometry (IM-MS). Samples were prepared at a final peptide concentration of 10 μM in 10 mM ammonium acetate, pH 7.4. The samples were analyzed on a home-built ion mobility spectrometry−mass spectrometer.[89] Briefly, for ion-mobility measurements, ions are generated continuously by a nano-ESI source, focused and stored in the ion funnel. A pulse of ions is injected into a temperature-controlled drift cell filled with helium gas (3−5 Torr), in which the ions move under the influence of a weak electric field. The injection energy can be varied from ∼20 to 150 eV, but it is usually kept as low as possible to minimize thermal heating of the ions during the injection process. After exiting the drift cell, the ions are further analyzed with a quadrupole mass filter, detected by the conversion dynode and channel electron multiplier, and recorded as a function of their arrival time distribution (ATD). The ATD can be related to the time the ions spend in the drift cell, which is directly related to the ion mobility and collision cross-section (σ) of the ion.[90] The measured σ provides information about the three-dimensional configurations of the ion. The width of the ATD can be compared to the width calculated for a single ion structure,[90] which gives information on the structural distribution favored in the ATD. If a feature in the experimental ATD is broader than the calculated one, then the feature may represent a family of structures rather than a single structure.

Oligomerization of Aβ42 by PICUP. Aβ oligomerization was monitored using photo-induced cross-linking of unmodified proteins (PICUP), essentially as described.[26,91] Briefly, peptide samples were prepared, as described in Peptide Synthesis and Preparation, to produce final peptide concentrations in the range of 25−35 μM. Then 18 μL of sample were periodically subjected to the PICUP reaction.[91] Briefly, 1 μL of 2 mM Tris (2,2′-bipyridyl)dichlororuthenium(II) hexahydrate (Ru(bpy)) was added to a 0.2 mL thin-walled PCR tube (Eppendorf AG, Hamburg, Germany) containing the peptide, followed by addition of 1 μL of 40 mM ammonium persulfate (APS) in phosphate buffer. The tube then was irradiated for 1 s with incandescent light using a high intensity illuminator (150 W, Dolan-Jenner Industries Inc., model 170-D). The reaction was quenched immediately with 1 μL of 1 M DTT in water, and then the sample was vortexed and placed on ice. To determine the oligomer size distribution, an equal volume of 2× Tris-Tricine SDS sample buffer (Invitrogen, Carlsbad, CA) was added to each sample. The samples then were boiled in a 100 °C water bath for 10 min and electrophoresed on a 10−20% T, 1 mm thick, Tris-Tricine SDS gel (Invitrogen, Carlsbad, CA). Silver staining was done using X-Press silver staining.

Quasielastic Light Scattering Spectroscopy (QLS). *Mm*, *Od*, and Aβ42 were dissolved at a concentration of 0.5 mg/mL in phosphate buffer, briefly vortexed, sonicated for 20 s, and filtered using a 20 nm Anotop filter (Whatman, Maidstone, England). Samples were monitored at ≈22 °C for 7−10 days. Measurements were done using a custom optical setup comprising a 40 mW He−Ne laser (λ = 633 nm) (Coherent, Santa Clara, CA) and PD2000DLS detector/correlator unit (Precision Detectors, Bellingham, MA). Light scattering was measured at a 90° angle. The intensity correlation function and the diffusion coefficient (D) frequency distribution were determined using

DOI: 10.1021/acschemneuro.5b00180
ACS Chem. Neurosci. XXXX, XXX, XXX−XXX

Precision Deconvolve software (Precision Detectors, Bellingham, MA). Hydrodynamic radius R_H was calculated from D according to the Stokes–Einstein–Sutherland equation $R_H = k_B T/6\pi\eta D$; where k_B is Boltzmann's constant, T is Kelvin, and η is the solvent viscosity.[92]

To determine the instrument-independent rate of change in relative intensity, we calculate the normalized quantity $(dI/dt)/I_0$ (units of h^{-1}, where h is hours). The rate of change in scattering intensity, dI/dt, was determined by fitting to a linear function spanning the first hour of incubation. I_0 was determined from the derived line $I_t = (dI/dt)t + I_0$ by substitution of $t = 0$. Both dI/dt and I_0 depend on the aperture in which light is collected, which in turn is a function of the instrument used. We note that these quantities are precise, but likely not absolutely accurate, because the intensity versus time dependency over this time interval is significantly nonlinear.

Bis-ANS Fluorescence. 1,1′-Bis(4-anilino,5-naphthalene sulfonic acid (Bis-ANS)) fluorescence was monitored periodically in 20 μM Aβ42 samples incubating at 37 °C with shaking (160 rpm). Then 50 μL of the sample (5 μM final concentration in the cuvette) was removed at regular intervals and added to 150 μL of 133.3 μM Bis-ANS solution in a 1.5 mL semi-micro disposable fluorescence cuvette (Brand, Germany). The cuvette was placed in the dark at room temperature (RT; 22.5 °C) for 5 min without shaking and then fluorescence (λ_{ex} = 400 nm and λ_{em} = 495 nm) was determined using a Hitachi model F-4500 fluorescence spectrophotometer (Hitachi America, NJ). The excitation and emission slit widths were both 5 nm. Each sample was read in triplicate, averaged, and corrected using a buffer blank incubated for the same amount of time. The samples were read at 2 h intervals for the first 12 h and subsequently at 24 h intervals. The data were plotted in KaleidaGraph (v 4.1, Synergy Software, Reading, PA). Statistical analyses on the data (*t*-test and Mann–Whitney Rank test) were performed using SigmaStat (Jandel Scientific, San Jose, CA).

Circular Dichroism Spectroscopy. *Mm*, *Od*, and Aβ42 peptides were prepared from HFIP dried films at final concentrations of 20 μM. The peptides were incubated in 1 mm path length cuvettes, without shaking, at 37 °C. Spectra were acquired using a JASCO J-810 spectropolarimeter (Tokyo, Japan) every 15 min for the first 3 h and subsequently every 30–60 min. CD measurement parameters were: wavelength range, 190–260 nm; data pitch, 0.2 nm; continuous scan mode; scan speed, 100 nm/min; response time, 1 s; bandwidth, 2 nm; scan number per sample, 7. The raw spectra were smoothed using the means movement smoothing parameters within the data acquisition software (Spectra Manager 2). The data were subsequently plotted in KaleidaGraph (v 4.1, Synergy Software, Reading, PA).

Electron Microscopy (EM). Formvar 400 mesh grids were glow discharged on a Med010 mini-deposition system EM glow discharge attachment model BU007284-T (Balzers Union Ltd., Hudson, NH) containing a cylindrical discharge compartment and an adjacent discharge control and timer unit. Then 8 μL aliquots of samples were examined immediately after dissolution (≈0.5 h) and at the end of assembly (7 d). The assembly process occurred during sample incubation at 37 °C with continuous shaking (160 rpm). Samples were mixed gently before application to the grids, after which the grid was covered and incubated for 20 min at RT. Liquid was wicked off carefully using a filter paper wick by gently touching the tip of the filter paper to the edge of the grid. Then 5 μL of 2.5% (v/v) glutaraldehyde in water were added to the grid, which then was incubated for 3 min in the dark. The glutaraldehyde solution was wicked off and replaced with 5 μL of 1% (w/v) uranyl acetate in water, which then was incubated for 3 min in the dark. The grids then were wicked off and air-dried. A JEOL 1200 EX (JEOL Ltd., Tokyo, Japan; 40–120 kV) transmission electron microscope was used to visualize the samples.[93]

Neuronal Cell Cultures. Primary cortical or hippocampal neurons were prepared as described previously.[94] Briefly, pregnant E18 rats were euthanized with CO_2 and the pups were removed immediately. Brains were dissected in chilled Leibovitz's L-15 medium, pH 7.5 (ATCC, Manassas, VA), in the presence of 1 μg/mL penicillin/streptomycin (Invitrogen, Carlsbad, CA). The tissue was incubated with 0.25% (w/v) trypsin in phosphate-buffered saline, pH 7.5 (PBS), containing 0.02% (w/v) EDTA for 30 min and then mechanically dissociated in a small volume of Leibovitz's L-15 medium using a fire-polished Pasteur pipet. The neurons were suspended in Dulbecco's Modified Eagle's Medium, pH 7.5 (DMEM; ATCC), containing 10% (v/v) heat-inactivated fetal bovine serum (FBS) (ATCC) and penicillin/streptomycin (1 μg/mL) and plated on poly-D-lysine (0.1 mg/mL, Sigma) coated 96-well COSTAR plates (Corning, Lowell, MA) at a density of 3×10^5 cells/mL. Then 24 h after the cells had been plated, the medium was replaced with fresh medium supplemented with 5 μM cytosine β-D-arabinofuranoside (Sigma Chemical Co, St Louis, MO) to inhibit the proliferation of glial cells. The cultures were maintained for 6 d before being treated with Aβ42. PC-12 cells were cultured and differentiated with 50 ng/mL nerve growth factor (NGF) 24 h prior to treatment with peptides, as described previously.[49] SHSY-5Y cells were grown in DMEM/F12K (1:1) media, pH 7.5, containing 10% (v/v) heat-inactivated FBS and penicillin/streptomycin (1 μg/mL), 2 mM glutamine, and 1.5 g/L sodium bicarbonate. The cultures were maintained at 37 °C in a humidified atmosphere of 5% (v/v) CO_2.

MTT (3-(4,5-Dimethylthiazol-2-yl)-2,5-diphenyltetrazolium bromide) Assay. Cell metabolism was evaluated using the MTT assay, as described previously.[95] Briefly, rat primary cortical neurons or NGF-differentiated PC12 cells were treated with 10 μM freshly prepared Aβ42 for 24 h at 37 °C. A 24 h incubation period produces a system with a robust ability to reveal neurotoxic effects. Following treatment, 15 μL of MTT, prepared by dissolution in 10% (v/v) Triton-X 100 in 2-propanol containing 0.1 N HCl, according to the manufacturer's instructions (Promega, Madison, WI), was added to each well and the samples were incubated for 4 h at 37 °C. "Stop solution" (Promega, Madison, WI) then was added, and the samples were incubated overnight at RT. OD was measured using a Synergy plate reader (Bio-TEK Instruments, Winooski, VT). A minimum of three independent experiments (six wells per data point) was performed. Data were normalized to the medium control group and expressed as the mean ± the standard error of the mean (SEM). Percent cell viability V was determined according to the formula:

$$V = \left[1 - \frac{OD_{sample} - OD_{medium}}{OD_{staurosporine} - OD_{medium}}\right] \times 100$$

where OD_{sample}, $OD_{staurosporine}$, and OD_{medium} correspond to the reference corrected OD values ($OD_{570} - OD_{630}$) of the sample, the staurosporine "100% kill" control, and the medium (cell-free) control. Reference corrected values take into account the absorbance maximum for the formazan product of MTT (570 nm) and scattering (630 nm), which can be caused by adventitious particles, fingerprints, or other purely technical reasons and can be interpreted incorrectly as absorbance.

LDH (Lactate Dehydrogenase) Assay. LDH assays were used to assess membrane integrity, as described previously.[93] Briefly, rat primary cortical neurons and NGF-differentiated PC12 cells were incubated with 10 μM Aβ42 peptide for 48 h at 37 °C in Eagle's Minimal Essential Medium (MEM, Earle's Salts, supplied glutamine-free) supplemented with 5% (v/v) heat-inactivated horse serum, 5% (v/v) fetal bovine serum, 2 mM glutamine, and 25 mM glucose. A 48 h incubation period produces a system with a robust ability to reveal neurotoxic effects. Percent toxicity was calculated, as detailed in the CytoTox-ONE homogeneous membrane integrity assay (Promega) instruction manual, according to the formula:

$$T = (F_{sample} - F_{med})/(F_{max} - F_{med}) \times 100$$

where T is percent toxicity, F_{sample} is sample fluorescence at 590 nm, F_{med} is fluorescence of medium alone, and F_{max} is maximum LDH release determined by treatment of the cells with staurosporine (1 μM final concentration). Data from a minimum of three independent experiments (six wells per data point) were normalized to media control and expressed as mean ± SEM.

Apoptosis Assay. Apoptosis was estimated using Annexin V-FITC fluorescence. Briefly, SH-SY5Y neuroblastoma cells (ATCC CRL-2266) were grown on microscopy slide coverslips coated with poly D-

DOI: 10.1021/acschemneuro.5b00180
ACS Chem. Neurosci. XXXX, XXX, XXX–XXX

lysine (0.1 mg/mL) in DMEM/F12K (1:1) medium containing 10% (v/v) heat-inactivated fetal bovine serum (FBS), penicillin/streptomycin (1 μg/mL), 2 mM glutamine, and 1.5 g/L sodium bicarbonate. The cells were maintained at 37 °C in a humidified atmosphere of 5% (v/v) CO_2 in air until a cell density of 1−5 × 10^5 cells per well was obtained, at which point the cells were exposed to peptide (final concentration 10 μM) for 24 h. The peptides were prepared by dissolution of lyophilizates in HFIP, at a concentration of ∼1 mg/mL, in 1.5 mL V-bottom polypropylene microcentrifuge tubes (Eppendorf, Fisher Scientific). This volume, which varied depending on peptide weight, is considered "1 v". Peptide "films" were produced by covering the open tubes with Kimwipes to prevent dust accumulation and placing the tubes in a chemical fume hood overnight to allow HFIP evaporation to occur. Immediately prior to use, the HFIP films were dissolved in 1 v of 60 mM sodium hydroxide, sonicated for 1 min, and then admixed with 9 v of culture medium to produce a peptide concentration of 100 μM. Then 200 μL of this solution were added to 60 mm diameter Petri dishes containing the coverslips on which the neurons were grown, followed by the addition of 1.8 mL of fresh DMEM/F12K medium. Quantitative amino acid analysis has shown that the peptide concentration within the HFIP/peptide solution or within the resolubilized peptide films was identical, within experimental error. Staurosporine (1 μM final concentration) was added to cells as a positive control for apoptosis. The negative control was cells treated with medium containing no Aβ42. After the incubation period, the coverslip was washed in PBS and fixed with 4% (v/v) paraformaldehyde in PBS. The cells were stained with an Annexin V-FITC apoptosis detection kit (Bio Vision Incorporated, Milpitas, CA) according to the manufacturer's instructions. Images were recorded using a confocal laser scanning microscope (Zeiss, model LSM 700; λ_{ex} = 488 nm and λ_{em} = 535 nm). The numbers of apoptotic cells were counted in a 100 μm^2 area using Image-J software (Image-J, NIH). A minimum of 30 microscopic fields was used for morphometric analysis from two independent experiments.

■ ASSOCIATED CONTENT

Supporting Information

The Supporting Information is available free of charge on the ACS Publications website at DOI: 10.1021/acschemneuro.5b00180.

Collision cross-sections of Aβ monomers and oligomers (PDF)

Oligomer distributions of non-cross-linked peptides; secondary structure dynamics (PDF)

■ AUTHOR INFORMATION

Corresponding Author

*Phone: 310-206-2030. Fax: 310-206-1700. E-mail: dteplow@mednet.ucla.edu.

Present Address

⊥For P.M.: Field Neuroscience Institute, St. Mary Hospital and Central Michigan University, 4677 Towne Center Road, Suite no. 101, Saginaw, Michigan 48604, United States.

Funding

This work was supported by NIH grants NS038328 (DBT), AG041295 (DBT), AG047116 (MTB), and by the Jim Easton Consortium for Drug Discovery and Biomarkers at UCLA (D.B.T. and G.B.).

Notes

The authors declare no competing financial interest.

■ ACKNOWLEDGMENTS

We acknowledge the use of instruments at the Electron Imaging Center for Nano Machines at the California Nano Systems Institute, UCLA (supported by NIH grant 1S10RR23057). The original idea for this project was provided by Dr. Dennis Selkoe to DBT.

■ ABBREVIATIONS USED

Aβ, amyloid β-protein; Aβ42, amyloid β-protein (1−42); AD, Alzheimer's disease; IM-MS, Ion mobility−mass spectrometry; *Mm*, *Mus musculus* Aβ42; PICUP, photo-induced cross-linking of unmodified proteins; *Ru (Bpy)*, tris(2,2′-bipyridyl)dichloro ruthenium(II) hexahydrate; *Od*, *Octodon degus* Aβ42

■ REFERENCES

(1) Selkoe, D. J. (2001) Alzheimer's disease: genes, proteins, and therapy. *Physiol. Rev. 81*, 741−766.

(2) Selkoe, D. J. (2013) SnapShot: Pathobiology of Alzheimer's disease. *Cell 154*, 468−468.

(3) Albert, M. S. (2011) Changes in cognition. *Neurobiol. Aging 32* (Suppl 1), S58−S63.

(4) Selkoe, D. J. (2000) The genetics and molecular pathology of Alzheimer's disease - Roles of amyloid and the presenilins. *Neurol Clin 18*, 903−922.

(5) Selkoe, D. J. (1997) Alzheimer's disease: genotypes, phenotypes, and treatments. *Science 275*, 630−631.

(6) Johnstone, E. M., Chaney, M. O., Norris, F. H., Pascual, R., and Little, S. P. (1991) Conservation of the sequence of the Alzheimer's disease amyloid peptide in dog, polar bear and five other mammals by cross-species polymerase chain reaction analysis. *Mol. Brain Res. 10*, 299−305.

(7) Selkoe, D. J. (1989) Biochemistry of altered brain proteins in Alzheimer's disease. *Annu. Rev. Neurosci. 12*, 463−490.

(8) Selkoe, D. J., Bell, D. S., Podlisny, M. B., Price, D. L., and Cork, L. C. (1987) Conservation of brain amyloid proteins in aged mammals and humans with Alzheimer's disease. *Science 235*, 873−877.

(9) Inestrosa, N. C., Reyes, A. E., Chacon, M. A., Cerpa, W., Villalon, A., Montiel, J., Merabachvili, G., Aldunate, R., Bozinovic, F., and Aboitiz, F. (2005) Human-like rodent amyloid-β-peptide determines Alzheimer pathology in aged wild-type Octodon degu. *Neurobiol. Aging 26*, 1023−1028.

(10) van Groen, T., Kadish, I., Popovic, N., Popovic, M., Caballero-Bleda, M., Bano-Otalora, B., Vivanco, P., Rol, M. A., and Madrid, J. A. (2011) Age-related brain pathology in Octodon degu: Blood vessel, white matter and Alzheimer-like pathology. *Neurobiol. Aging 32*, 1651−1661.

(11) Ardiles, A. O., Tapia-Rojas, C. C., Mandal, M., Alexandre, F., Kirkwood, A., Inestrosa, N. C., and Palacios, A. G. (2012) Postsynaptic dysfunction is associated with spatial and object recognition memory loss in a natural model of Alzheimer's disease. *Proc. Natl. Acad. Sci. U. S. A. 109*, 13835−13840.

(12) Tarragon, E., Lopez, D., Estrada, C., Ana, G. C., Schenker, E., Pifferi, F., Bordet, R., Richardson, J. C., and Herrero, M. T. (2013) Octodon degus: A model for the cognitive impairment associated with Alzheimer's disease. *CNS Neurosci. Ther. 19*, 643−648.

(13) Edrey, Y. H., Medina, D. X., Gaczynska, M., Osmulski, P. A., Oddo, S., Caccamo, A., and Buffenstein, R. (2013) Amyloid beta and the longest-lived rodent: the naked mole-rat as a model for natural protection from Alzheimer's disease. *Neurobiol. Aging 34*, 2352−2360.

(14) Edrey, Y. H., Oddo, S., Cornelius, C., Caccamo, A., Calabrese, V., and Buffenstein, R. (2014) Oxidative damage and amyloid-β metabolism in brain regions of the longest-lived rodents. *J. Neurosci. Res. 92*, 195−205.

(15) Otvos, L., Jr., Szendrei, G. I., Lee, V. M., and Mantsch, H. H. (1993) Human and rodent Alzheimer β-amyloid peptides acquire distinct conformations in membrane-mimicking solvents. *Eur. J. Biochem. 211*, 249−257.

(16) Hilbich, C., Kisters-Woike, B., Reed, J., Masters, C. L., and Beyreuther, K. (1991) Human and rodent sequence analogs of Alzheimer's amyloid βA4 share similar properties and can be solubilized in buffers of pH 7.4. *Eur. J. Biochem. 201*, 61−69.

DOI: 10.1021/acschemneuro.5b00180
ACS Chem. Neurosci. XXXX, XXX, XXX−XXX

(17) Fung, J., Frost, D., Chakrabartty, A., and McLaurin, J. (2004) Interaction of human and mouse Aβ peptides. *J. Neurochem. 91*, 1398−1403.
(18) Janssen, J. C., Beck, J. A., Campbell, T. A., Dickinson, A., Fox, N. C., Harvey, R. J., Houlden, H., Rossor, M. N., and Collinge, J. (2003) Early onset familial Alzheimer's disease: Mutation frequency in 31 families. *Neurology 60*, 235−239.
(19) Ono, K., Condron, M. M., and Teplow, D. B. (2010) Effects of the English (H6R) and Tottori (D7N) familial Alzheimer disease mutations on amyloid β-protein assembly and toxicity. *J. Biol. Chem. 285*, 23186−23197.
(20) De Strooper, B., Simons, M., Multhaup, G., Van Leuven, F., Beyreuther, K., and Dotti, C. G. (1995) Production of intracellular amyloid-containing fragments in hippocampal neurons expressing human amyloid precursor protein and protection against amyloidogenesis by subtle amino acid substitutions in the rodent sequence. *EMBO J. 14*, 4932−4938.
(21) Dyrks, T., Dyrks, E., Masters, C. L., and Beyreuther, K. (1993) Amyloidogenicity of rodent and human βA4 sequences. *FEBS Lett. 324*, 231−236.
(22) Fraser, P. E., Nguyen, J. T., Inouye, H., Surewicz, W. K., Selkoe, D. J., Podlisny, M. B., and Kirschner, D. A. (1992) Fibril formation by primate, rodent, and Dutch-hemorrhagic analogues of Alzheimer amyloid β-protein. *Biochemistry 31*, 10716−10723.
(23) Teplow, D. B., Lazo, N. D., Bitan, G., Bernstein, S., Wyttenbach, T., Bowers, M. T., Baumketner, A., Shea, J. E., Urbanc, B., Cruz, L., Borreguero, J., and Stanley, H. E. (2006) Elucidating Amyloid β-Protein Folding and Assembly: A Multidisciplinary Approach. *Acc. Chem. Res. 39*, 635−645.
(24) Teplow, D. B. (2006) Preparation of amyloid β-protein for structural and functional studies. *Methods Enzymol. 413*, 20−33.
(25) Bernstein, S. L., Wyttenbach, T., Baumketner, A., Shea, J. E., Bitan, G., Teplow, D. B., and Bowers, M. T. (2005) Amyloid β-protein: monomer structure and early aggregation states of Aβ42 and its Pro19 alloform. *J. Am. Chem. Soc. 127*, 2075−2084.
(26) Bitan, G., and Teplow, D. B. (2004) Rapid photochemical cross-linking—a new tool for studies of metastable, amyloidogenic protein assemblies. *Acc. Chem. Res. 37*, 357−364.
(27) Einstein, A. (1905) The motion of elements suspended in static liquids as claimed in the molecular kinetic theory of heat. *Ann. Phys. 322*, 549−560.
(28) Sutherland, W. (1905) A dynamical theory of diffusion for non-electrolytes and the molecular mass of albumin. *Philos. Mag. 9*, 781−785.
(29) Lomakin, A., Chung, D. S., Benedek, G. B., Kirschner, D. A., and Teplow, D. B. (1996) On the nucleation and growth of amyloid β-protein fibrils: detection of nuclei and quantitation of rate constants. *Proc. Natl. Acad. Sci. U. S. A. 93*, 1125−1129.
(30) Lomakin, A., Benedek, G. B., and Teplow, D. B. (1999) Monitoring protein assembly using quasielastic light scattering spectroscopy. *Methods Enzymol. 309*, 429−459.
(31) Rosen, C. G., and Weber, G. (1969) Dimer formation from 1-amino-8-naphthalenesulfonate catalyzed by bovine serum albumin. A new fluorescent molecule with exceptional binding properties. *Biochemistry 8*, 3915−3920.
(32) Hawe, A., Sutter, M., and Jiskoot, W. (2008) Extrinsic fluorescent dyes as tools for protein characterization. *Pharm. Res. 25*, 1487−1499.
(33) Horowitz, P., Prasad, V., and Luduena, R. F. (1984) Bis(1,8-anilinonaphthalenesulfonate). A novel and potent inhibitor of microtubule assembly. *J. Biol. Chem. 259*, 14647−14650.
(34) Liu, Y., and Schubert, D. (1997) Cytotoxic amyloid peptides inhibit cellular 3-(4,5-dimethylthiazol-2-yl)-2,5-diphenyltetrazolium bromide (MTT) reduction by enhancing MTT formazan exocytosis. *J. Neurochem. 69*, 2285−2293.
(35) Abe, K., and Kimura, H. (1996) Amyloid β toxicity consists of a Ca^{2+}-independent early phase and a Ca^{2+}-dependent late phase. *J. Neurochem. 67*, 2074−2078.
(36) Wyttenbach, T., and Bowers, M. (2003) Gas-Phase Conformations: The Ion Mobility/Ion Chromatography Method in *Modern Mass Spectrometry, Topics in Current Chemistry* (Schalley, C. A., Ed.), pp 207−232, Springer, Berlin, Heidelberg.
(37) Baumketner, A., Bernstein, S. L., Wyttenbach, T., Bitan, G., Teplow, D. B., Bowers, M. T., and Shea, J. E. (2006) Amyloid β-protein monomer structure: a computational and experimental study. *Protein Sci. 15*, 420−428.
(38) Bernstein, S. L., Dupuis, N. F., Lazo, N. D., Wyttenbach, T., Condron, M. M., Bitan, G., Teplow, D. B., Shea, J. E., Ruotolo, B. T., Robinson, C. V., and Bowers, M. T. (2009) Amyloid-β protein oligomerization and the importance of tetramers and dodecamers in the aetiology of Alzheimer's disease. *Nat. Chem. 1*, 326−331.
(39) Bleiholder, C., Dupuis, N. F., Wyttenbach, T., and Bowers, M. T. (2011) Ion mobility-mass spectrometry reveals a conformational conversion from random assembly to β-sheet in amyloid fibril formation. *Nat. Chem. 3*, 172−177.
(40) Gessel, M. M., Bernstein, S., Kemper, M., Teplow, D. B., and Bowers, M. T. (2012) Familial Alzheimer's disease mutations differentially alter amyloid β-protein oligomerization. *ACS Chem. Neurosci. 3*, 909−918.
(41) Gessel, M. M., Wu, C., Li, H., Bitan, G., Shea, J. E., and Bowers, M. T. (2012) Aβ39−42) modulates Aβ oligomerization but not fibril formation. *Biochemistry 51*, 108−117.
(42) Zheng, X., Gessel, M. M., Wisniewski, M. L., Viswanathan, K., Wright, D. L., Bahr, B. A., and Bowers, M. T. (2012) Z-Phe-Ala-diazomethylketone (PADK) disrupts and remodels early oligomer states of the Alzheimer disease Aβ42 protein. *J. Biol. Chem. 287*, 6084−6088.
(43) Roychaudhuri, R., Lomakin, A., Bernstein, S., Zheng, X., Condron, M. M., Benedek, G. B., Bowers, M., and Teplow, D. B. (2014) Gly25-Ser26 amyloid β-protein structural isomorphs produce distinct Aβ42 conformational dynamics and assembly characteristics. *J. Mol. Biol. 426*, 2422−2441.
(44) Lee, S., Zheng, X., Krishnamoorthy, J., Savelieff, M. G., Park, H. M., Brender, J. R., Kim, J. H., Derrick, J. S., Kochi, A., Lee, H. J., Kim, C., Ramamoorthy, A., Bowers, M. T., and Lim, M. H. (2014) Rational design of a structural framework with potential use to develop chemical reagents that target and modulate multiple facets of Alzheimer's disease. *J. Am. Chem. Soc. 136*, 299−310.
(45) Zheng, X., Liu, D., Klarner, F. G., Schrader, T., Bitan, G., and Bowers, M. T. (2015) Amyloid β-protein assembly: The effect of molecular tweezers CLR01 and CLR03. *J. Phys. Chem. B 119*, 4831−4841.
(46) Lesné, S., Koh, M. T., Kotilinek, L., Kayed, R., Glabe, C. G., Yang, A., Gallagher, M., and Ashe, K. H. (2006) A specific amyloid-β protein assembly in the brain impairs memory. *Nature 440*, 352−357.
(47) Bitan, G., Kirkitadze, M. D., Lomakin, A., Vollers, S. S., Benedek, G. B., and Teplow, D. B. (2003) Amyloid β-protein (Aβ) assembly: Aβ40 and Aβ42 oligomerize through distinct pathways. *Proc. Natl. Acad. Sci. U. S. A. 100*, 330−335.
(48) Lomakin, A., and Teplow, D. B. (2012) Quasielastic light scattering study of amyloid β-protein fibrillogenesis in *Methods in Molecular Biology* (Sigurdsson, E. M., Calero, M., and Gasset, M. A., Eds.), pp 69−83, Springer Science + Business Media, New York.
(49) Fradinger, E. A., Monien, B. H., Urbanc, B., Lomakin, A., Tan, M., Li, H., Spring, S. M., Condron, M. M., Cruz, L., Xie, C. W., Benedek, G. B., and Bitan, G. (2008) C-terminal peptides coassemble into Aβ42 oligomers and protect neurons against Aβ42-induced neurotoxicity. *Proc. Natl. Acad. Sci. U. S. A. 105*, 14175−14180.
(50) Stryer, L. (1965) The interaction of a naphthalene dye with apomyoglobin and apohemoglobin: A fluorescent probe of non-polar binding sites. *J. Mol. Biol. 13*, 482−495.
(51) Rosen, C. G., and Weber, G. (1969) Dimer formation from 1-anilino-8-naphthalenesulfonate catalyzed by bovine serum albumin. A new fluorescent molecule with exceptional binding properties. *Biochemistry 8*, 3915−3920.
(52) Semisotnov, G. V., Rodionova, N. A., Razgulyaev, O. I., Uversky, V. N., Gripas', A. F., and Gilmanshin, R. I. (1991) Study of the "molten

DOI: 10.1021/acschemneuro.5b00180
ACS Chem. Neurosci. XXXX, XXX, XXX−XXX

globule" intermediate state in protein folding by a hydrophobic fluorescent probe. *Biopolymers 31*, 119−128.
(53) Shi, L., Palleros, D. R., and Fink, A. L. (1994) Protein conformational changes induced by 1,1′-Bis(4-anilino-5-naphthalene-sulfonic acid): preferential binding to the molten globule of DnaK. *Biochemistry 33*, 7536−7546.
(54) Lansbury, P. T., Jr. (1999) Evolution of amyloid: what normal protein folding may tell us about fibrillogenesis and disease. *Proc. Natl. Acad. Sci. U. S. A. 96*, 3342−3344.
(55) Fezoui, Y., and Teplow, D. B. (2002) Kinetic studies of amyloid β-protein fibril assembly. Differential effects of α-helix stabilization. *J. Biol. Chem. 277*, 36948−36954.
(56) Drake, A. F. (1994) Circular Dichroism in *Methods in Molecular Biology: Microscopy, Optical Spectroscopy, and Macroscopic Techniques* (Jones, B. M. C. and Thomas A. H., Ed.), pp 219−244, Humana Press Inc, Totowa, NJ.
(57) Fasman, G. D. (1996) *Circular Dichroism and the Conformational Analysis of Biomolecules*; Plenum Press, New York, London.
(58) Matsuo, K., Sakurada, Y., Yonehara, R., Kataoka, M., and Gekko, K. (2007) Secondary-structure analysis of denatured proteins by vacuum-ultraviolet circular dichroism spectroscopy. *Biophys. J. 92*, 4088−4096.
(59) Walsh, D. M., Lomakin, A., Benedek, G. B., Condron, M. M., and Teplow, D. B. (1997) Amyloid β-protein fibrillogenesis. Detection of a protofibrillar intermediate. *J. Biol. Chem. 272*, 22364−22372.
(60) Broersen, K., Rousseau, F., and Schymkowitz, J. (2010) The culprit behind amyloid beta peptide related neurotoxicity in Alzheimer's disease: oligomer size or conformation? *Alzheimer's Res. Ther. 2*, 12.
(61) Vermes, I., Haanen, C., Steffens-Nakken, H., and Reutellingsperger, C. (1995) A novel assay for apoptosis. Flow cytometric detection of phosphatidylserine expression on early apoptotic cells using fluorescein labelled Annexin V. *J. Immunol. Methods 184*, 39−51.
(62) Aubry, J. P., Blaecke, A., Lecoanet-Henchoz, S., Jeannin, P., Herbault, N., Caron, G., Moine, V., and Bonnefoy, J. Y. (1999) Annexin V used for measuring apoptosis in the early events of cellular cytotoxicity. *Cytometry 37*, 197−204.
(63) Dahlgren, K. N., Manelli, A. M., Stine, W. B., Jr., Baker, L. K., Krafft, G. A., and LaDu, M. J. (2002) Oligomeric and fibrillar species of amyloid-β peptides differentially affect neuronal viability. *J. Biol. Chem. 277*, 32046−32053.
(64) Klein, W. L., Stine, W. B., Jr., and Teplow, D. B. (2004) Small assemblies of unmodified amyloid β-protein are the proximate neurotoxin in Alzheimer's disease. *Neurobiol. Aging 25*, 569−580.
(65) Larson, M. E., and Lesne, S. E. (2012) Soluble Aβ oligomer production and toxicity. *J. Neurochem. 120* (Suppl s1), 125−139.
(66) Anfinsen, C. B. (1973) Principles that govern the folding of protein chains. *Science 181*, 223−230.
(67) Eichner, T., and Radford, S. E. (2011) A diversity of assembly mechanisms of a generic amyloid fold. *Mol. Cell 43*, 8−18.
(68) Burdick, D., Soreghan, B., Kwon, M., Kosmoski, J., Knauer, M., Henschen, A., Yates, J., Cotman, C., and Glabe, C. (1992) Assembly and aggregation properties of synthetic Alzheimer's A4/β amyloid peptide analogs. *J. Biol. Chem. 267*, 546−554.
(69) Valerio, M., Porcelli, F., Zbilut, J. P., Giuliani, A., Manetti, C., and Conti, F. (2008) pH effects on the conformational preferences of amyloid β-peptide (1−40) in HFIP aqueous solution by NMR spectroscopy. *ChemMedChem 3*, 833−843.
(70) Crescenzi, O., Tomaselli, S., Guerrini, R., Salvadori, S., D'Ursi, A. M., Temussi, P. A., and Picone, D. (2002) Solution structure of the Alzheimer amyloid β-peptide (1−42) in an apolar microenvironment. Similarity with a virus fusion domain. *Eur. J. Biochem. 269*, 5642−5648.
(71) Hamley, I. W. (2012) The amyloid beta peptide: a chemist's perspective. Role in Alzheimer's and fibrillization. *Chem. Rev. 112*, 5147−5192.
(72) Harrison, R. S., Sharpe, P. C., Singh, Y., and Fairlie, D. P. (2007) Amyloid peptides and proteins in review. *Rev. Physiol Biochem Pharmacol 159*, 1−77.
(73) Devanathan, S., Salamon, Z., Lindblom, G., Grobner, G., and Tollin, G. (2006) Effects of sphingomyelin, cholesterol and zinc ions on the binding, insertion and aggregation of the amyloid Aβ1−40 peptide in solid-supported lipid bilayers. *FEBS J. 273*, 1389−1402.
(74) Yip, C. M., and McLaurin, J. (2001) Amyloid-β peptide assembly: a critical step in fibrillogenesis and membrane disruption. *Biophys. J. 80*, 1359−1371.
(75) Yip, C. M., Darabie, A. A., and McLaurin, J. (2002) Aβ42-peptide assembly on lipid bilayers. *J. Mol. Biol. 318*, 97−107.
(76) Muchowski, P. J., and Wacker, J. L. (2005) Modulation of neurodegeneration by molecular chaperones. *Nat. Rev. Neurosci. 6*, 11−22.
(77) Mawuenyega, K. G., Sigurdson, W., Ovod, V., Munsell, L., Kasten, T., Morris, J. C., Yarasheski, K. E., and Bateman, R. J. (2010) Decreased clearance of CNS β-amyloid in Alzheimer's disease. *Science 330*, 1774.
(78) Bates, K. A., Verdile, G., Li, Q. X., Ames, D., Hudson, P., Masters, C. L., and Martins, R. N. (2009) Clearance mechanisms of Alzheimer's amyloid-β peptide: implications for therapeutic design and diagnostic tests. *Mol. Psychiatry 14*, 469−486.
(79) Wang, Y.-J., Zhou, H.-D., and Zhou, X.-F. (2006) Clearance of amyloid-β in Alzheimer's disease: progress, problems and perspectives. *Drug Discovery Today 11*, 931−938.
(80) Guenette, S. Y. (2003) Mechanisms of Aβ clearance and catabolism. *NeuroMol. Med. 4*, 147−160.
(81) Tanzi, R. E., Moir, R. D., and Wagner, S. L. (2004) Clearance of Alzheimer's Aβ peptide: the many roads to perdition. *Neuron 43*, 605−608.
(82) Yamada, T., Sasaki, H., Furuya, H., Miyata, T., Goto, I., and Sakaki, Y. (1987) Complementary DNA for the mouse homolog of the human amyloid beta protein precursor. *Biochem. Biophys. Res. Commun. 149*, 665−671.
(83) De Strooper, B., Van Leuven, F., and Van den Berghe, H. (1991) The amyloid β protein precursor or proteinase nexin II from mouse is closer related to its human homolog than previously reported. *Biochim. Biophys. Acta, Gene Struct. Expression 1129*, 141−143.
(84) Lehman, E. J., Kulnane, L. S., Gao, Y., Petriello, M. C., Pimpis, K. M., Younkin, L., Dolios, G., Wang, R., Younkin, S. G., and Lamb, B. T. (2003) Genetic background regulates β-amyloid precursor protein processing and β-amyloid deposition in the mouse. *Hum. Mol. Genet. 12*, 2949−2956.
(85) Mitsuda, N., Roses, A. D., and Vitek, M. P. (1997) Transcriptional Regulation Of the Mouse Presenilin-1 Gene. *J. Biol. Chem. 272*, 23489−23497.
(86) Duyckaerts, C., Potier, M. C., and Delatour, B. (2008) Alzheimer disease models and human neuropathology: similarities and differences. *Acta Neuropathol. 115*, 5−38.
(87) Borchelt, D. R., Ratovitski, T., Vanlare, J., Lee, M. K., Gonzales, V., Jenkins, N. A., Copeland, N. G., Price, D. L., and Sisodia, S. S. (1997) Accelerated amyloid deposition in the brains of transgenic mice coexpressing mutant presenilin 1 and amyloid precursor proteins. *Neuron 19*, 939−945.
(88) Rahimi, F., Maiti, P., and Bitan, G. (2009) Photo-induced cross-linking of unmodified proteins (PICUP) applied to amyloidogenic peptides. *J. Visualized Exp.* No. 23, e1071.
(89) Wyttenbach, T., Kemper, P. R., and Bowers, M. T. (2001) Design of a new electrospray ion mobility mass spectrometer. *Int. J. Mass Spectrom. 212*, 13−23.
(90) Mason, E. A., and McDaniel, E. W. (1988) *Transport Properties of Ions in Gases*; Wiley, New York.
(91) Bitan, G. (2006) Structural study of metastable amyloidogenic protein oligomers by photo-induced cross-linking of unmodified proteins. *Methods Enzymol. 413*, 217−236.
(92) Einstein, A. (1905) Über die von der molekularkinetischen Theorie der Wärme geforderte Bewegung von in ruhenden Flüssigkeiten suspendierten Teilchen. *Ann. Phys. 322*, 549−560.
(93) Roychaudhuri, R., Yang, M., Deshpande, A., Cole, G. M., Frautschy, S., Lomakin, A., Benedek, G. B., and Teplow, D. B. (2013)

DOI: 10.1021/acschemneuro.5b00180
ACS Chem. Neurosci. XXXX, XXX, XXX−XXX

C-terminal turn stability determines assembly differences between Aβ40 and Aβ42. *J. Mol. Biol. 425*, 292−308.
(94) Maiti, P., Piacentini, R., Ripoli, C., Grassi, C., and Bitan, G. (2011) Surprising toxicity and assembly behaviour of amyloid β-protein oxidized to sulfone. *Biochem. J. 433*, 323−332.
(95) Ono, K., Condron, M. M., and Teplow, D. B. (2009) Structure-neurotoxicity relationships of amyloid β-protein oligomers. *Proc. Natl. Acad. Sci. U. S. A. 106*, 14745−14750.

DOI: 10.1021/acschemneuro.5b00180
ACS Chem. Neurosci. XXXX, XXX, XXX−XXX

Oligomer	Charge state	*Aβ42*		*Od*		*Mm*	
		σ	**σ/n**	**σ**	**σ/n**	**σ**	**σ/n**
Monomer	-2	-	-	-	-	618	618
	-3 (M_1)	643	643	630	630	635	635
	-3 (M_2)	702	702	692	692	698	698
	-3 (M_3)	-	-	-	-	757	757
	-4	792	792	790	790	807	807
Dimer	-4	-	-	-	-	968	484
	-5	1246	623	1218	609	1234	617
Trimer	-6	-	-	-	-	1275	425
Tetramer	-10	2172	543	2156	539	2204	551
Hexamer	-15	2838	473	2928	488	2910	485
Dodecamer	-30	4560	380	4512	376	-	-

Table S1. Collision cross-sections (σ; in $Å^2$) of Aβ monomers and oligomers. σ/n represents the cross-section of each monomer within an oligomer. The error for the cross-sections is ≈0-1%.

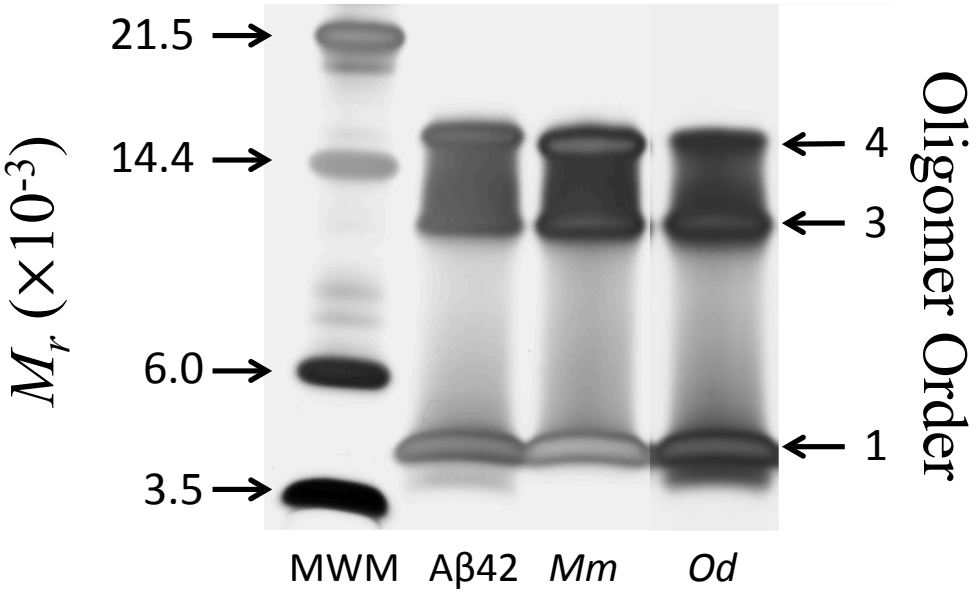

Figure S1: Oligomer distributions of non-cross-linked peptides. An aliquot of each freshly prepared peptide was electrophoresed in a 10-20% gradient Tricine-SDS gel. Bands were visualized by silver staining. Oligomer order is indicated by numbers and arrows on the right. We note an increase in trimer versus tetramer in the Od lane relative to the other lanes. This could indicate preferential formation of trimers by Od. (All lanes are from the same gel, but an irrelevant intervening lane has been deleted from the figure.)

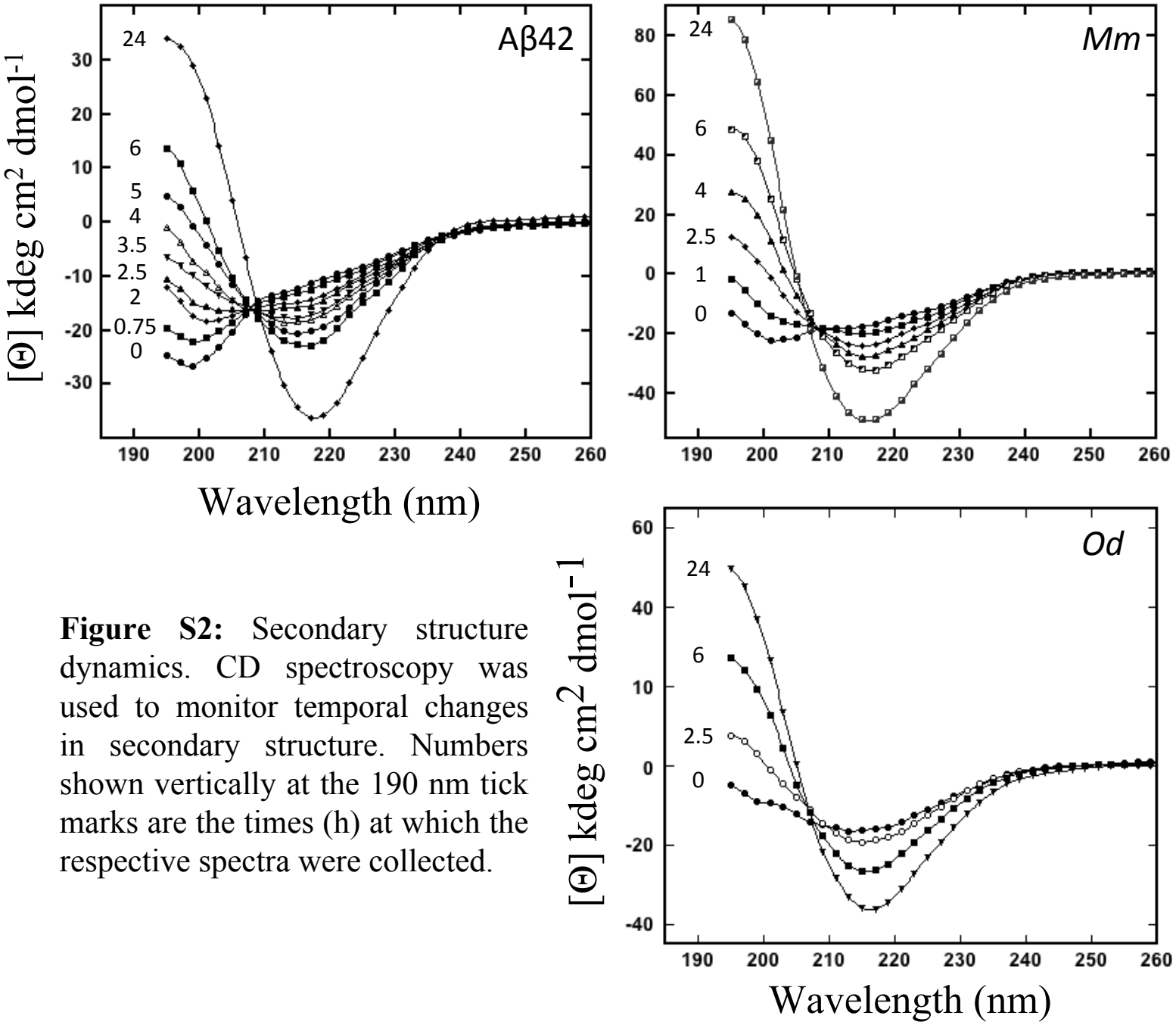

Figure S2: Secondary structure dynamics. CD spectroscopy was used to monitor temporal changes in secondary structure. Numbers shown vertically at the 190 nm tick marks are the times (h) at which the respective spectra were collected.